AD NUMBER

AD815946

NEW LIMITATION CHANGE

TO

Approved for public release, distribution unlimited

FROM

Distribution: No Foreign

AUTHORITY

US Navy Underwater Sound Lab notice dtd 15 May 1979

AD815946

Report on the Status of Project AMOS

(Acoustic, Meteorological, and Oceanographic Survey)

(1 January 1953 - 31 December 1954)

H. Wysor Marsh, Jr.
Morris Schulkin

9 May 1967

U. S. Navy Underwater Sound Laboratory
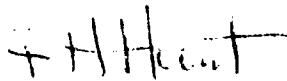Fort Trumbull, New London, Connecticut

AD815946

ABSTRACT

This report is an UNCLASSIFIED edition of USL Report No. 255 (CONFIDENTIAL), dated 21 March 1955. The Project AMOS work which was carried out through the period 1 January 1953 - 31 December 1954 is summarized. This is a final report of the AMOS deep-water acoustic measurements, which began in June 1949. During the period covered by this report, the Underwater Sound Laboratory carried out a number of studies and analyses of AMOS data; these are included herein as Studies A through D and H through J.

The major study is an analysis of sound transmission at frequencies between 2 and 25 kc based on all the AMOS data and on other data available in the literature. Propagation-loss prediction charts based on this analysis are presented as a function of certain environmental parameters. An error study of the propagation analysis is presented next. Studies of AMOS low-frequency noisemaker data analysis, ray tracing in the ocean, and bottom reflection in deep water are also presented, and a summary of Cruise TWELVE, which was completed early in this period, is included.

ADMINISTRATIVE INFORMATION

REVIEWED AND APPROVED: 9 May 1967

F. H. Hunt
Associate Technical Director for Administration

TABLE OF CONTENTS

i

TABLE OF CONTENTS (Cont'd)

LIST OF ILLUSTRATIONS

LIST OF ILLUSTRATIONS (Cont'd)

LIST OF TABLES

v

Fig. 1 - Project AMOS Cruises from 1949 through 1953

REPORT ON THE STATUS OF PROJECT AMOS
(Acoustic, Meteorological, and Oceanographic Survey)
(1 January 1953 – 31 December 1954)

INTRODUCTION

Project AMOS (Acoustic, Meteorological, and Oceanographic Survey) was established in order to permit the collection of acoustic propagation data and the simultaneous observation of meteorological and oceanographic factors of significance to sonar performance in the vital sea lanes of the Atlantic Ocean during all seasons of the year. The information obtained was designed to cover both current and planned echo-ranging and listening frequencies.

The major objectives of Project AMOS have been achieved in one form or another. It is planned to make continued use of the Project AMOS propagation-loss data and environmental statistics for operational studies as indicated. The AMOS objectives are the following:

a. The preparation of a set of prediction charts for operational planning purposes. Such charts represent the sonar situation on a probability basis for each area of interest and for each month of the year. Various sets of charts corresponding to equipment categories, such as surface-ship-mounted echo-ranging sonar, variable-depth echo-ranging sonar, or submarine-installed low-frequency passive sonar, may be prepared. From these charts, it will be possible to determine not only the probability of achieving a particular detection range on a submarine by echo-ranging or listening but also the probable range of detection of a convoy by an enemy submarine.

b. The compilation of a set of detailed prediction charts for tactical employment, based upon the propagation loss and figure of merit for particular sonar equipments in relation to the prevailing oceanographic conditions. These charts will be used for day-to-day operations, for convoy screen spacing, and for similar applications.

c. The formulation of a set of design charts which will make possible intelligent design of sonar equipment to meet specified operational requirements.

The participants in the AMOS program were the U. S. Navy Hydrographic Office and the U. S. Navy Underwater Sound Laboratory. Jointly they were responsible for acquiring simultaneous acoustic and environmental data. The Underwater Sound Laboratory was responsible for the design, installation, and operation of acoustic equipment, while the Hydrographic Office carried out the design, installation, and operation of oceanographic and meteorological equipment. These agencies were also jointly responsible for the development of methods and techniques for field utilization and for presentation of the acoustic-oceanographic data to the Forces Afloat. This responsibility involved the preparation and publication of material which provides procedures for converting equipment characteristics and local environmental conditions into operationally and tactically usable terms.

In addition to acquiring acoustic data, the Laboratory undertook the analysis and correlation of simultaneously observed acoustic and environmental data for operational purposes. The Hydrographic Office was responsible for the acquisition and analysis of extensive environmental data for operational purposes and for the publication of operational sonar charts. It also was responsible for the preliminary planning of AMOS cruises, handled such matters as itineraries, project coordination, time and space allotments, personnel assignments, proposed shipyard installation of scientific equipment, and the preparation of technical instructions, and initiated "working-level" conferences with the agencies and vessels involved.

SUMMARY OF ACCOMPLISHMENTS OF PROJECT AMOS

This report is a final report of the AMOS acoustic-environmental correlations in deep water. The Underwater Sound Laboratory is now undertaking an extensive program of shallow-water propagation

1

measurements.[1] A summary of the accomplishments of Project AMOS at the Underwater Sound Laboratory is now included.

Since the inception of the AMOS program, a sizable amount of acoustic propagation data has been accumulated for the North Atlantic Ocean for a wide range of acoustic frequencies and environmental conditions. The map in Fig. 1 shows the ten joint oceanographic and acoustic stations for which propagation-loss data have been obtained up through Cruise TWELVE. The AMOS cruises in which the Laboratory participated are listed below:

AMOS Cruises

AMOS Cruise Number	Cruise Date	Acoustic Stations Occupied
TWO	June 1949	6
THREE	July-September 1949	29
FOUR	October-December 1949	17
FIVE	February-May 1950	23
SEVEN	November-December 1950	7
EIGHT	February-April 1951	30
NINE	June-September 1951	20
TEN	January-April 1952	18
ELEVEN	June-September 1952	20
TWELVE	February-April 1953	20
		192

The propagation-loss data obtained on these cruises were punched on IBM cards as indicated below. Finally a set of 26,672 IBM cards was prepared for all AMOS cruises with four-frequency (2.2, 8, 16, and 25 kc) propagation-loss data at standard projector depths, receiver depths, and ranges. Copies of most of these cards have been furnished to the Naval Research Laboratory and the University of Michigan. Available transmission data cover a frequency range of from 70 cps to 25 kc, and vertical reverberation measurements cover the range from 2.2 to 34 kc. A list of propagation-run station positions is given in Tables 1A and 1B for both high-frequency and low-frequency runs.

All North Atlantic and Mediterranean BT observations in the Woods Hole Oceanographic Institution File through November 1951 have been re-duced to IBM cards and tabulated.[2] Copies of the tabulations have been furnished to the Woods Hole Oceanographic Institution, the Navy Hydrographic Office, and the Agricultural and Mechanical College of Texas. There are 131,600 pairs of cards in the North Atlantic File and 14,550 pairs of cards in the Mediterranean File. This set of environmental data cards has proved to be quite important in a number of applications. The cards have been separated into various geographical areas, and statistical compilations of important factors have been made. The Hydrographic Office has agreed to keep this basic file up to date and recently shipped 48,000 cards to the Laboratory.

Acoustic propagation and associated environmental data obtained from AMOS cruises are inventoried below.

AMOS Acoustic Cards		AMOS BT Card File	
(Card Layout Form, Fig. 7, USL Report No. 147)		(Card Layout Form, Fig. 8, USL Report No. 147)	
Cruise	No. of Cards	Cruise	No. of Cards
2	750 ⎫ 21, 25, 29 kc	2	50
3	4,750 ⎭	5	250
5	3,000 ⎫	3	350
7	500 ⎬ 8, 16, 25 kc	7	50
8	15,000 ⎭	8	400
9	13,050 ⎫	9	400
10	16,000 ⎪	10	450
11	22,000 ⎬ 2.2,8,16,25 kc	11	550
12	12,500 ⎭	12	250
Total	88,050		2,750

Hydrographic Office AMOS Cruise Oceanographic Station File
(Data for all cruises have been received in listing form.)
(Card Layout Forms, Figs. 14-15, USL Report No. 147)

Cruise	No. of Cards
1	5100
2	650
3	2700
4	2400
5	2250

[1] The present status of the shallow-water measurements program is covered in USL Report No. 260, Quarterly Report, 1 July - 30 September 1954 (CONFIDENTIAL).

[2] The IBM cards used for this purpose are shown in Fig. 1 of USL Report No. 147, Report on the Status of Project AMOS (20 April - 31 December 1951), by H. W. Marsh, Jr., and M. Schulkin, 19 February 1952 (CONFIDENTIAL).

2

Table 1

PROJECT AMOS PROPAGATION RUN STATIONS IN DEEP WATER

A. High Frequency [2,2, 8, 16, 25 (21, 29) kc]

Cruise	Acoustic Station	Date (start)	Latitude	Longitude	Water Depth (fm)	Hydrographic Station No.
2	1	18 VI 49	39°42'N	70°34'W	1340	53-1
	2	19 VI 49	38°17'N	69°25'W	1900	53-2
	3	19 VI 49	36°53'N	68°17'W	2530	53-3
	4	22 VI 49	36°53'N	62°05'W	2500	52-5
	5	22 VI 49	36°53'N	55°55'W	2800	53-6
	7	26 VI 49	43°12'N	60°00'W	890	52-9
3	3	16 VII 49	30°33'N	59°56'W	2800	55-2
	6	17 VII 49	30°13.5'N	54°28'W	2960	54-3
	9	18 VII 49	30°33'N	48°55'W	2620	55-5
	12	20 VII 49	30°51.3'N	43°17.5'W	1720	54-6
	15	21 VII 49	31°07'N	37°42'W	1850	55-8
	18	22 VII 49	31°24'N	32°04.8'W	2400	54-9
	21	23 VII 49	31°37.1'N	28°30.2'W	2825	55-11
	24	25 VII 49	31°57.5'N	20°49.0'W	2600	54-12
	27	26 VII 49	32°13.4'N	15°26.0'W	2340	55-14
	32	28 VII 49	34°24.2'N	7°35.1'W	710	54-16
	36	31 VII 49	36°05.0'N	9°43.1'W	2170	54-19
	39	1 VIII 49	38°23'N	10°25.5'W	2650	55-19
	42	8 VIII 49	40°49.5'N	13°49.5'W	2800	54-22
	45	10 VIII 49	44°56.5'N	16°11.5'W	2400	55-21
	48	11 VIII 49	46°44'N	12°44'W	2250	54-25
	50	12 VIII 49	47°49'N	10°18'W	2095	54-26
	54	19 VIII 49	51°11'N	14°35.1W	330	54-28
	57	20 VIII 49	52°06.8'N	20°21'W	2040	54-30
	60	21 VIII 49	53°04.6'N	26°16.8'W	1900	54-32
	63	22 VIII 49	53°52'N	31°54'W	1440	55-29
	66	23 VIII 49	50°43.2'N	31°13'W	1850	54-34
	69	25 VIII 49	47°19.5'N	30°26.5'W	1850	--
	72	26 VIII 49	43°45.5'N	29°09'W	1600	54-37
	75	29 VIII 49	39°10'N	27°43'W	645	55-35
	78	2 IX 49	37°11.8'N	32°04.9'W	1200	54-40
	81	3 IX 49	36°31.8'N	38°51.2'W	1750	55-38
	84	5 IX 49	36°14.5'N	44°50.1'W	2500	54-43
	87	6 IX 49	34°43.6'N	51°26.6'W	2390	55-41
	90	7 IX 49	35°06.8'N	58°03.5'W	2480	54-46
5	1	15 II 50	34°41.8'N	70°00.6'W	--	58-2
	2	18 II 50	26°12.1'N	69°08.0'W	--	--
	3	22 II 50	16°33.0'N	66°33.1'W	2350	--
	4	23 II 50	12°16.0'N	62°50.0'W	1600	58-9
	5	28 II 50	11°28.0'N	59°19.8'W	1010	58-10
	6	1 III 50	16°19.3'N	58°28.2'W	2930	58-11
	7	3 III 50	21°16.2'N	57°54.1'W	2770	59-20
	8	5 III 50	26°20.1'N	57°08.1'W	3000	58-14
	9	6 III 50	31°18.0'N	56°28.2'W	2965	59-23
	10	8 III 50	36°15.5'N	55°56.5'W	2850	58-17
	11	10 III 50	41°16.5'N	55°08.5'W	2850	59-25
	12	16 III 50	41°53.1'N	50°03.9'W	2000	58-21
	13	17 III 50	38°53.5'N	44°28.0'W	2775	59-28

(Continued)

Table 1 (Cont'd)

Cruise	Acoustic Station	Date (start)	Latitude	Longitude	Water Depth (fm)	Hydrographic Station No.
5	14	19 III 50	35°23.0'N	37°15.2'W	1560	59-30
	15	20 III 50	35°13.6'N	33°46.3'W	1390	59-31
	16	23 III 50	36°22.0'N	29°59.0'W	1700	59-32
	17	28 III 50	42°31.5'N	22°45.2'W	2000	59-34
	18	30 III 50	46°41.0'N	18°38.0'W	2400	59-36
	19	31 III 50	49°50.0'N	15°00.2'W	2490	59-37
	20	28 IV 50	19°32.2'N	22°51.0'W	2180	59-60
	21	30 IV 50	24°52.4'N	28°19.5'W	3000	58-35
	22	4 V 50	30°02.5'N	35°10.0'W	2210	59-63
	23	6 V 50	29°56.2'N	42°59.3'W	1660	59-65
	24	8 V 50	30°49.6'N	52°08.3'W	2850	59-67
	25	10 V 50	31°57.9'N	60°58.0'W	2620	58-40
7	2	23 XI 50	29°11.0'N	70°20.0'W	2860	--
	3	26 XI 50	19°32.0'N	67°55.0'W	2000	62-1
	5	28 XI 50	14°14.8'N	72°14.7'W	1800	63-4
	6	29 XI 50	13°31.1'N	75°23.5'W	2100	63-5
	7	1 XII 50	17°11.6'N	81°12.9'W	710	63-7
	8	3 XII 50	23°35.4'N	83°53.6'W	1200	63-9
8	1	4 II 51	31°23.9'N	67°32.1'W	2750	65-1
	2	6 II 51	30°24.5'N	61°8.0'W	2800	65-3
	3	8 II 51	30°38.5'N	53°15.5'W	3020	55-4
	4	9 II 51	30°23.0'N	49°9.0'W	2500	65-5
	7	15 II 51	30°25.0'N	36°44.0'W	2300	64-9
	8	18 II 51	31°55.0'N	22°59.0'W	2850	65-11
	9	20 II 51	32°49.0'N	18°35.0'W	1880	64-11
	10	21 II 51	33°57.0'N	13°19.0'W	2400	64-12
	11	22 II 51	35°27.0'N	7°33.0'W	750	64-13
	12	4 III 51	36°00.0'N	10°12.0'E	250	65-17
	13	6 III 51	35°23.0'N	22°39.0'E	2040	64-18
	14	9 III 51	36°52.0'N	18°2.0'E	1970	64-19
	15	11 III 51	39°03.0'N	14°31.0'E	1850	65-21
	16	12 III 51	41°38.0'N	10°25.0'E	800	64-21
	17	22 III 51	37°41.0'N	00°30.0'E	1300	65-26
	18	27 III 51	39°43.0'N	11°19.0'W	2240	64-26
	19	29 III 51	44°39.0'N	7°56.0'W	2620	64-27
	20	11 IV 51	46°54.4'N	9°32.0'W	500	65-31
	21	12 IV 51	46°25.0'N	12°10.0'W	2250	65-32
	22	13 IV 51	43°00.0'N	18°40.0'W	2350	64-33
	23	19 IV 51	32°34.0'N	30°55.0'W	2250	64-36
	24	21 IV 51	32°37.0'N	36°47.0'W	1740	64-37
	25	25 IV 51	32°50.0'N	53°39.0'W	2550	65-41
	26	27 IV 51	32°46.0'N	59°06.0'W	2640	64-41
9	1	2 VII 51	41°20.0'N	59°16.0'W	2600	66-2
	3	4 VII 51	44°42.0'N	47°23.0'W	2000	67-4
	4	6 VII 51	49°49.5'N	43°15.0'W	2250	67-6
	5	8 VII 51	54°2.0'N	38°15.0'W	1480	66-8
	6	9 VII 51	56°51.0'N	34°58.0'W	1000	67-8
	7	12 VII 51	58°19.0'N	33°13.0'W	950	67-9
	8	14 VII 51	62°20.0'N	27°37.0'W	800	67-10
	9	20 VII 51	59°39.0'N	22°46.0'W	1300	66-13
	10	22 VII 51	54°1.0'N	21°0.0'W	1500	66-15
	11	24 VII 51	45°22.3'N	19°24.2'W	2300	67-15
	12	26 VII 51	40°15.0'N	18°52.0'W	3000	67-16
	13	2 VIII 51	38°35.4'N	16°24.1'W	2950	67-18
	14	3 VIII 51	41°47.6'N	15°59.8'W	2875	66-21
	15	4 VIII 51	44°1.3'N	15°48.6'W	3000	67-19
	16	6 VIII 51	46°25.6'N	15°18.0'W	2400	66-22
	17	7 VIII 51	50°18.7'N	14°37.7'W	2300	66-23

(Continued)

4

Table 1 (Cont'd)

Cruise	Acoustic Station	Date (start)	Latitude	Longitude	Water Depth (fm)	Hydrographic Station No.
9	19	8 VIII 51	55°21.5'N	11°43.5'W	1500	66-24
	20	5 IX 51	43°21.8'N	29°53.7'W	1760	67-25
10	1	30 II 52	47°42.0'N	43° 1.0'W	2100	68-1
	2	2 II 52	54° 9.0'N	34°34.0'W	1150	68-2
	3	4 II 52	58°00.0'N	29° 5.0'W	1260	68-4
	4	5 II 52	60°43.0'N	25°00.0'W	1100	68-6
	5	8 II 52	56°24.0'N	10°42.0'W	1350	68-7
	6	10 II 52	54°58.0'N	12°20.0'W	1600	68-9
	7	11 II 52	57°00.0'N	12°27.0'W	1215	68-10
	8	21 II 52	61°21.0'N	10°36.0'W	650	68-14
	9	27 II 52	65° 1.0'N	2°36.0'W	1680	68-16
	10	28 II 52	63°45.0'N	0°17.5'W	1300	69-17
	11	7 III 52	60° 7.0'N	5°57.0'W	610	68-18
	13	16 III 52	44°57.0'N	13°37.0'W	1900	68-23
	15	24 III 52	39°15.0'N	14°40.0'W	2520	69-25
	16	26 III 52	40°21.0'N	23°18.0'W	2270	69-27
	17	30 III 52	41°24.0'N	41° 9.0'W	2600	68-30
	18	1 IV 52	41°59.0'N	47°44.0'W	2010	69-28
11	1	14 VI 52	42°35.0'N	58° 7.0'W	1450	—
	2	16 VI 52	49° 8.0'N	48°37.0'W	1200	70-1
	3	18 VI 52	56° 5.0'N	41°40.0'W	1920	71-2
	4	20 VI 52	59°59.0'N	34°11.0'W	1330	70-4
	5	22 VI 52	62° 9.0'N	22°20.0'W	870	70-6
	6	23 VI 52	62°16.0'N	15°25.0'W	1200	70-7
	7	24 VI 52	61°16.0'N	10°39.0'W	630	71-7
	8	8 VII 52	66°22.0'N	3°23.0'E	840	71-11
	9	11 VII 52	70° 3.0'N	15°45.0'E	1300	70-34
	10	14 VII 52	73°39.0'N	8°59.0'E	1350	70-38
	11	16 VII 52	70°28.0'N	8° 2.0'E	1610	70-39
	12	18 VII 52	75°32.0'N	0°53.0'E	960	71-42
	13	20 VII 52	73°47.0'N	10° 9.0'W	1700	70-44
	14	21 VII 52	72°19.0'N	3°31.0'W	1330	71-45
	15	23 VII 52	68°55.0'N	4° 1.0'E	1810	71-46
	16	29 VII 52	66°12.0'N	3°33.0'E	820	71-47
	17	1 VIII 52	68°14.0'N	1°13.0'W	1960	71-73
	18	20 VIII 52	55°36.0'N	11°43.0'W	1550	71-82
	21	26 VIII 52	50°55.0'N	41°42.0'W	2350	71-88
12	2	15 II 53	42°38.0'N	60°35.0'W	1840	72-2
	4	18 II 53	35°53.4'N	62°44.2'W	2750	73-6
	5	19 II 53	34°14.2'N	63° 6.7'W	2750	72-3
	6	3 III 53	27° 7.5'N	57°10.0'W	3510	73-9
	7	3 III 53	26°00.0'N	58°54.1'W	3360	72-6
	8	5 III 53	22°40.8'N	57°12.9'W	3350	73-10
	9	7 III 53	19°23.0'N	58°57.0'W	2620	72-8
	10	9 III 53	17° 6.2'N	58°49.4'W	2975	73-14
	11	16 III 53	14°47.1'N	59°30.0'W	1680	72-12
	12	18 III 53	12°24.0'N	60°32.2'W	1350	72-14
	13	19 III 53	14°31.8'N	60°18.5'W	1370	73-19
	14	20 III 53	16°41.0'N	60°42.0'W	3000	72-17
	15	22 III 53	18°20.0'N	62° 9.0'W	2840	72-18
	16	3 IV 53	25°55.5'N	67°30.0'W	2940	73-26
	17	4 IV 53	24°32.1'N	69°19.0'W	3050	72-21
	18	5 IV 53	26°25.1'N	69°51.1'W	2975	73-27
	19	6 IV 53	25°14.0'N	71°38.7'W	3000	72-22
	20	7 IV 53	27° 6.1'N	72°15.9'W	2760	73-28
	21	15 IV 53	29°41.1'N	75°14.1'W	2565	73-30
	22	16 IV 53	31°41.1'N	76° 7.5'W	1500	73-31

B. Low Frequency

Date*	Latitude	Longitude	Broad-Band Source†		Bomb Drop Range (kyd)	Hydrophone Depth (ft)
			Type	Range (kyd)		
18 VII 52	75°00'N	1°00'E	Siren	0.5-70	70	50; 500
1 VIII 52	68°00'N	1°00'W	Siren	0.5-70	70	50; 500
14 II 53	42°25'N	60°32'W	Mk 4v	0.5-33	42	--; 500
19 II 53	35° 7'N	62°56'W	Siren	0.5-40	80	--; 500
20 II 53	33°59'N	63°23'W	Mk 4v	0.5-80	80	--; 500
21 II 53	30°18'N	64°37'W	Mk 4v	{ 70-9	9	50; 500
				9-49	49	50; 500
23 II 53	32°22'N	65° 9'W	None	--	80	--; 500
4 III 53	25°35'N	58°56'W	None	--	87	50; 500
8 III 53	18°13'N	56°54'W	None	--	65	50; 500
10 III 53	15°17'N	59°34'W	None	--	86	--; 500
18 III 53	12°47'N	60°35'W	Siren	0.5-14	78	--; 500
21 III 53	16°49'N	60°43'W	None	--	80	50; 500
29 III 53	18°31'N	66° 5'W	Mk 4v	6.0-90	90	50; 500
30 III 53	18°31'N	66° 5'W	Mk 4v	4.0-70	70	--; 500
31 III 53	18°31'N	66° 5'W	Mk 4v	2.0-53	53	50; 500
3 IV 53	29°51'N	67°28'W	Mk 4v	0.5-54	54	50; 500
4 IV 53	24°32'N	69°24'W	None	--	80	50; 500
5 IV 53	26°24'N	69°52'W	Mk 4v	0.5-80	80	50; --
6 IV 53	25°20'N	71°39'W	Mk 4v	0.5-76	76	50; --
9 IV 53	25°58'N	73°26'W	Mk 4v	0.5-65	65	50; --
13 IV 53	25°27'N	76°15'W	Mk 4v	>30-80	80	50; --
16 IV 53	29°36'N	75°24'W	Mk 4v	0.5-80	80	--; 500
20 IV 53	38° 4'N	73°54'W	Mk 4v	0.5-74	74	50; --
20 IV 53	36°24'N	72°50'W	Mk 4v	0.5-88	88	50; --
21 IV 53	37°36'N	72°55'W	Mk 4v	0.5-90	90	50; --
22 IV 53	38°23'N	72°58'W	Mk 4v	0.5-75	75	50; --

* Stations conducted on 18 VII 52 and 1 VIII 52 were occupied on Cruise ELEVEN. All other stations occupied on Cruise TWELVE.

† All Siren and Mk 4v noisemaker runs have been processed.

..In addition, all the wartime acoustic and environmental records of the University of California Division of War Research have been transcribed on IBM cards. The shallow-water propagation surveys made in Fishers Island Sound by the Columbia University Division of War Research and the East Coast and Gulf of Mexico shallow-water propagation surveys carried out by WHOI have been transcribed to punched-card form. An inventory of these propagation and environmental data in the Laboratory's IBM punched-card file is presented below:

UCDWR Acoustic Data
(Card Layout Forms, Figs. 9-12, USL Report No. 147)

		No. of Cards
Low Frequency:	Acoustic	1861
0.2, 0.6, 1.8, 7.5, and 22.5 kc	Environmental	436
High Frequency:	Acoustic	4112
10, 14, 20, 40, 56, and 60 kc but primarily 24 kc	Environmental	1541
		7950

Fishers Island Sound and Block Island Sound Shallow-Water Data
(Columbia University Division of War Research)

	Number
Environmental Cards	30
Acoustic Data Cards	100

Woods Hole Oceanographic Institution Shallow-Water Acoustic Data

	Number
Bathythermograph Cards	863
Environmental Cards	300
Acoustic Cards	500

During the year 1951, a set of QHBa performance charts was prepared. Included in this set were monthly tables and charts of expected sweep width for QHBa-equipped surface vessels for four operational submarine-depth intervals. Such strategic charts may be used in comparing convoy routes from the point of view of sonar protection and also for submarine operations.[3] This information was transmitted to the Hydrographic Office for publication and dissemination.[4]

In preparing these charts it was necessary to establish a QHBa figure-of-merit measurements program, which extended well into the year 1952.[5] As a result, the figures of merit of 27 destroyer-type ships of the Fleet were obtained under various environmental and ship operating conditions. Approximately 200 sonarmen participated in these operations. In addition to the data required for the strategic operational charts, many other important results were obtained from this figure-of-merit program. Significant personnel factors were uncovered, the importance of a clean sonar dome was emphasized, and the importance of a more rapid audio-beam search than that prescribed by QHBa doctrine was established.

An analysis was also made of the propagation data with respect to variable-depth sonar applications.[6] Project AMOS data were applied to the problem of determining the optimum depth for variable depth sonar and the gains to be expected for a system operating at this depth.

Another study carried out in the year 1952 concerned the expected operational performance of echo-ranging sonars at 5 kc and 10 kc.[7] In this work, aimed at efficient system design, Project AMOS propagation-loss data at acoustic frequencies of 2.2, 8, 16, 21, 25, and 29 kc were analyzed as a function of range and operational submarine-depth intervals for various BT AMOS code classes. A study was also made of the expected propagation-loss anomaly, at various ranges, arising from bottom-reflection acoustic paths in deep water. These propagation data were applied to monthly environmental statistics for the North Atlantic Ocean area between 30° N and 40° N in order to obtain the expected median range for four equipment figures of merit (140, 150, 160, and 170 db) for 5-kc and 10-kc, hull-mounted, echo-ranging sonar systems. In the present report, a modified version of this study has been prepared for systems at 8 and 14 kc.[8]

---

[3] Sample charts may be found in USL Report No. 147 (CONFIDENTIAL).

[4] See USL letter to the Hydrographic Office, "Status of Project AMOS," ser. 1110-036, 1 November 1951 (CONFIDENTIAL).

[5] This program is described by M. Schulkin, F. S. White, Jr., and R. A. Spong in QHBa Figure-of-Merit Tests, USL Report No. 187, 3 April 1953 (CONFIDENTIAL).

[6] See Appendix A of Report on the Status of Project AMOS (1 January - 31 December 1952), by H. W. Marsh, Jr., and M. Schulkin, USL Report No. 188, 3 April 1953 (CONFIDENTIAL).

[7] See USL Report No. 188 (CONFIDENTIAL), Appendix D.

[8] See Study F.

7

Bottom-reflection paths at these frequencies have been found to be less important than reported earlier.

Also in connection with this program a study concerned with the temperature dependence of attenuation was prepared.[9] The study of Project AMOS propagation measurements made in isothermal water shows that the temperature of the water has an important effect upon the propagation loss, the loss being greater in colder water.

In addition, propagation loss in isothermal layers depends slightly, but consistently, upon projector and receiver depths. Data which showed the distribution of propagation loss at frequencies from 2 to 25 kc, at ranges from 1 to 33 kyd, at projector and receiver depths from 20 to 500 ft, and at water temperatures from 35° F. to 70° F. were presented. The probable error under prescribed conditions was 3 db. The temperature effect is in good agreement with a model exhibiting a single relaxation process.[10] Also, a wave theoretical treatment of the propagation problem shows that certain features of the observed depth dependence are explicable.

Analyses of low-frequency noisemaker runs made on certain of the AMOS cruises were also carried out.[11] The purpose of these runs was to determine attenuation values for propagation of low-frequency (100 to 10,000 cps) sound under various oceanographic conditions. Topics of interest include propagation in surface channels, channeling of sound between the ocean surface and bottom, distances between focus points at various latitudes, and modification or design of equipment for better production and reception of low-frequency sound in the ocean.

The broad-band magnetic-tape records of low-frequency noisemakers are being processed with automatic equipment. The end product is a set of IBM punched cards, at approximately 250-yard intervals, which contain the measured level in ten frequency bands from approximately 200 cps to 10,000 cps; the actual frequencies depend on the source used. These runs can extend out to about 80 kyd, and background noise levels are entered

periodically in place of the noisemaker levels. Level-versus-range plots have been made for the card data by means of the automatic plotting machine. Range values were obtained from range-versus-travel time curves drawn from the bomb-drop data. Sound-velocity-versus-depth plots were completed for all deep Nansen cast data of Cruise TWELVE, and some ray computations were made therefrom.[12]

From the level-versus-range plots, levels have been read and tabulated for 0.25-kyd increments from 1 to 2 kyd, 0.5-kyd increments from 2.0 to 5.0 kyd, 1-kyd increments from 5 to 10 kyd, 2.5-kyd increments from 10 to 20 kyd, and 5-kyd increments from 20 kyd to the conclusion of the run. In the focus region, readings are tabulated at 0.25-kyd range increments.

Source levels for the two sources have been determined by assuming spherical spreading to 1000 yd for each station and extrapolating the value at 1000 yd back to 1 yd. An average value for each frequency band was then computed from the extrapolated values.

Plots of measured level plus computed spreading and absorption loss have been made against the grazing angle at the ocean bottom for frequencies of 1, 2, and 8 kc for those stations for which a reasonable estimate of the ranges at which bottom reflection paths predominate could be made.

An analysis of AMOS transmission data in the 2- to 25-kc frequency region, including propagation by way of the bottom, has been completed.[13] It is believed that, for the most part, propagation at these frequencies in deep water is fairly well understood in terms of environmental factors. In another report,[14] contours of transmission loss have been plotted for ten frequencies and three projector depths, for a standard temperature (50° F.) and a standard layer depth (100 ft). Correction charts have been plotted for each frequency for the correction required because of changes in layer depth, temperature, and sea state. Values for the absorption coefficient as a function of frequency and temperature are also included. These data have been used and will continue to be used in the future, in the frequency range covered, for

[9] See USL Report No. 188 (CONFIDENTIAL), Appendix C.

[10] A formula for the temperature effect on absorption including relaxation and viscous terms is presented in Study A of this report.

[11] See Studies I and J of this report.

[12] For the ray methods used, see Studies H and J of this report.

[13] See Study A.

[14] See Study B.

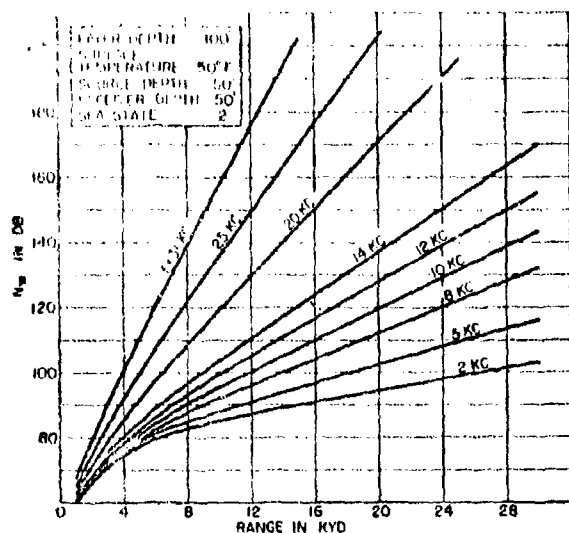Fig. 2 - Transmission Loss vs. Range for Standard
Conditions

Fig. 3 - Transmission Loss vs. Frequency for Standard
Conditions

operational applications involving echo-ranging, variable-depth sonar, and passive submarine sonar. It is important to have a standard reference of transmission loss related to range and frequency. Figures 2 and 3, applying to specific environmental conditions which are typical of those occurring naturally, are recommended for this purpose.

The AMOS propagation results were used to construct lateral range curves for hull-mounted, echo-ranging sonars at various frequencies and figures of merit for submarines at periscope depth and at the best depth for avoiding detection. [15] The curves apply to specific layer depths and surface temperatures. Such curves were used by CAPT S. D. B. Merrill to space the ships of his screen in AsDevEx-I. A subsequent study of AsDevEx-I and other available data showed that predicted and
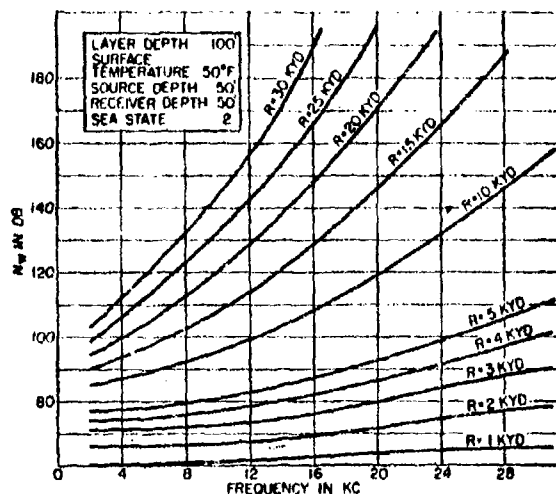
measured range performance compared favorably at all frequencies over a range of propagation conditions. [16]

As a result of its experience, the Laboratory has been assigned the problem of preparing a sonar range prediction manual to replace the existing manual, Sonar Prediction with the Bathythermograph (NAVSHIPS 900,111, 1 October 1947, CONFIDENTIAL). The Laboratory also plans to use its propagation information in the analysis of operational submarine array sonar contact reports. All such reports received to date have been keypunched, checked, and listed. Listings have been distributed to ComSubPac, ComSubLant, SubDevGruTWO, and Bureau of Ships.

---

[15] See Study E.

[16] See Study F. This study was delivered as a paper at the Ninth Navy Symposium on Underwater Acoustics, 17 June 1954, at the Naval Research Laboratory, Washington, D. C.

PROPAGATION ANALYSIS AND SONAR RANGE PREDICTIONS

The nine studies appended to this report represent work done on Project AMOS during the years 1953-54 in the fields of propagation analysis and sonar range predictions. Project AMOS collected

large quantities of propagation-loss data on extensive cruises to all parts of the North Atlantic in all seasons in order to extend our knowledge of propagation, both with respect to acoustic fre-

quency and depth of endpoint positions of the prop-
agation path. As each cruise was completed, the
data were examined and analyzed in the light of
previous cruise results, existing knowledge, and
contemporary research by other working groups. [17]

The final analysis, as given in Study A, was
considered to be consistent with information then
available. The propagation-loss data obtained from
AMOS cruises at discrete frequencies of 2.2, 8, 16,
and 25 kc were analyzed and interpreted according
to a definite model. Equations of propagation loss
were obtained for the model and fitted with semi-
empirical coefficients.

The steps used to arrive at this model con-
sisted of (1) finding the important acoustic-ocea-
nographic variables, (2) studying acoustic patterns
in situations when one of these variables domi-
nated, and (3) making the simplest assumptions re-
garding the acoustic interrelation of these varia-
bles and adding complications only when the
exigency of incorporating a large body of data into
the model so required.

The model was constructed from several modes
of propagation, each of which became important
under certain conditions of the wide range of geog-

raphy and season covered by the AMOS cruises.
While other observed effects could be included
readily, it was found that these occurred in an ex-
treme way only in certain localities. It was felt
that to introduce other parameters in order to take
these into account would unduly complicate the
analysis and would not improve the prediction ca-
pabilities for most of the localities and seasons.
In particular, the magnitude of the thermocline
gradient was an important variable of this type.
The propagation data for all thermocline gradients
were grouped in one class. In addition, the prop-
agation data for all temperature gradients more
positive than -0.3° F./100 ft were considered in
the mixed-layer class. It is recognized that these
assumptions must be modified for work in particular
localities.

The important oceanographic-acoustic varia-
bles for the frequencies under study were found to
be isothermal layer depth, temperature, and sea
state. The temperature effect was best studied in
the situation where a constant temperature pre-
vailed to very great depths. Under such conditions,
it was found that the acoustic field was generally
constant with depth at a fixed range out to ranges
of the order of 24 kyd, the limiting range of the ex-
perimental measurements. In such circumstances,
the attenuation constants were computed and plotted
against temperature for the four frequencies. These
data were then considered with respect to existing
data of the same kind and to other laboratory meas-
urements. The parameters of a theoretical expres-
sion involving the sum of a viscous contribution
and a relaxation phenomenon contribution were
then determined. Formula (7) of Study A represents
the resulting expression. Figures 10 and 11 of Study
B and Fig. 3 of Study A are graphs based on this
formula. It should be noted that the final value of
the relaxation coefficient is less than the value
0.76 presented in an earlier work. [18]

The next variable studied was isothermal layer
depth. In shallower layers than those considered
in the previous paragraph, there is a residual atten-
uation loss which depends on layer depth, range,
frequency, receiver and projector depth, and sea
state. It was quite obvious from the data that, at a
fixed range and projector and receiver depth, the
residual attenuation increased the higher the sea
state, the higher the frequency, and the shallower
the layer depth.

[17] Some of the reports and articles consulted during
the propagation analysis were: "Transmission," Part I,
Physics of Sound in the Sea, Summary Technical Re-
port of Division 6, NDRC, vol. 8, 1946 (UNCLASSI-
FIED); *Principles and Applications of Underwater
Sound*, Summary Technical Report of Division 6, NDRC,
vol. 7, 1946 (RESTRICTED); Sonar Data Division,
UCDWR., "The Influence of Thermal Conditions on the
Transmission of 24-kc Sound," UCDWR U307, 16 March
1945 (CONFIDENTIAL); R. J. Urick, "Sound Transmis-
sion Measurements at 8 and 16 kc in Caribbean Waters,
Spring 1949," NRL Report 3556, 11 November 1949
(CONFIDENTIAL); R. J. Urick, "Sound Transmission
Measurements in the Long-Island-Bermuda Region,"
NRL Report 3630, 6 September 1950 (CONFIDENTIAL);
R. J. Urick, "Sound Transmission to Long Ranges in
the Ocean," NRL Report 3729, 6 September 1950 (CON-
FIDENTIAL); H. R. Baker, A. G. Pieper, and C. W.
Searfoss, "Measurements of Sound Transmission Loss
at Low Frequencies 1.5 to 5 kc," NRL Report 4225,
23 September 1953 (CONFIDENTIAL); W. C. Meecham,
W. H. Kelly, J. R. Frederick, "An Investigation of the
Sound Transmission Loss in and below an Isothermal
Layer," Technical Report Project M936, 7 July 1953,
Engineering Research Institute University of Michigan
(CONFIDENTIAL); and J. R. Frederick, J. C. Johnson,
W. H. Kelly, "An Analysis of Underwater Sound Trans-
mission Data," Interim Technical Report, Project
M936, April 1954 (No. 1936-I-T), Engineering Research
Institute, University of Michigan (CONFIDENTIAL).

[18] See Appendix C, USL Report No. 188.

Thus, some kind of scattering phenomenon which depended directly on sea state, and inversely on volume, since a greater loss was observed for shallower layers, seemed to be operative. This could be explained most easily on the basis of a surface scattering phenomenon. A possible mechanism for volume scattering could be visualized whereby sea state somehow introduced volume scattering elements so that shallower layers had more intense scattering centers. Assuming that the mechanism is one of surface scattering, the loss can be related to the degree of contact that the acoustic energy has with the sea surface as well as to the size and frequency of the surface irregularities. For an omnidirectional source, the fraction of rays which are refracted upwards to meet the surface depends on the layer depth. The range of the limiting ray is a measure of this fraction. This range between successive surface contacts of the limiting ray turns out to be the $\sqrt{L}/2$ in kiloyards if L is expressed in feet. Thus, $\sqrt{L}$ is a suitable scaling factor for range if the degree of contact of energy with the surface is a satisfactory measure of the energy loss from a surface channel. By further scaling the projector and receiver depths to layer depth, it would seem possible to normalize the data for all layer depths at any single frequency. This was done in the analysis leading to Study A and proved to be a reliable way of translating a large amount of data into a single propagation class.

Three propagation zones were recognized in connection with propagation in the presence of isothermal layers. The near zone is defined by a limiting ray leaving a source and returning to the surface after touching the bottom of the surface channel. In this zone energy travels between points by a direct path and spreads spherically. In the far zone, energy is propagated down the channel after two or more contacts with the surface, and the decay of the acoustic field can be represented by a scattering loss coefficient added to the temperature absorption term at a fixed frequency. Cylindrical spreading holds in this region. The intermediate zone is a zone of transition between the near zone with spherical spreading and the far zone with cylindrical spreading and surface scattering loss. A semiempirical depth-loss factor was obtained for each zone, depending on the ratio of the scaled range in any zone to the scaled zone

width. The formulas provide a propagation loss for any projector-receiver depth pair.

When both ends of the propagation path are not in the isothermal layer, energy may penetrate below the layer by way of surface scattering, diffractive leakage from the surface channel, or diffractive leakage from the direct beam. The first two cases are taken care of by the depth-loss factor for each of the propagation zones of the previous mode.

The case of diffractive leakage from the direct beam must be treated individually when the mode of propagation involving downward refraction prevails. Downward refraction occurs in the presence of a negative velocity gradient directly below the surface when no layer is present or in the thermocline below an isothermal layer. Thus, when one end of the path is in the surface channel and one end is beneath the surface channel, this mode applies to the portion of the energy which is split at the limiting ray and is refracted downwards. The formulas for propagation loss for this mode have been based on a theoretical expression derived previously.[19] The term in the brackets of Formula (2) of Study A has been fitted with empirical coefficients for an average velocity gradient. The equation for the limiting ray under these conditions is:

$$ R = 1/5 \, \sqrt{|Z_0 - L|} + 1/5 \, \sqrt{|Z - L|} . $$

Since the acoustic intensity may be dominated either by leakage from the surface channel or diffracted energy from the downward refracted beam, computations must be made for both of these modes when both ends of the propagation path are not in the layer. The mode producing the lesser propagation loss is the one that prevails.

An important mode of propagation for variable-depth sonar applications occurs when a depressed or internal sound channel is present and both ends of the propagation path are in the channel. The axis of the channel is the depth of a sound velocity minimum. This condition usually occurs when the temperature gradient levels off below a steep thermocline and the pressure effect on sound velocity with increasing depth takes over. The SOFAR channel is such a case in point. It has

19 See H. W. Marsh, Jr., *Theory of the Anomalous Propagation of Acoustic Waves in the Ocean,* USL Report No. 111, 12 May 1950 (UNCLASSIFIED), p. 35.

been found from the AMOS data that for shallow, depressed channels the width of these channels is approximately equal to the depth of the channel axis. This model has been used to obtain an expression for the propagation loss, which is the same as that for the near zone of the surface channel. It should be noted that this expression holds on the average.

Finally, there are situations where energy is propagated between two points by way of the bottom. Data from several sources were combined to yield a set of curves of bottom loss versus bottom-grazing angle for frequencies from 125 cps to 32 kc. In using these curves, one calculates the spreading and absorption loss over the ray path for specular reflection on the bottom and inserts the appropriate bottom loss. For echo-ranging purposes, the one-way propagation loss computation must be doubled. Study D of this report presents a discussion of the data used in arriving at the bottom-loss curves.

An error analysis of the semiempirical formulas for computing propagation loss is given in Study C. It is shown there, on the basis of a sampling procedure, that the prediction method is reliable over the range of frequencies and ranges considered. Some reduction in probable error could be achieved perhaps for the downward refraction mode of propagation by taking the magnitude of the velocity

gradient into account, but this is hardly worth the additional complications.

Study F compares the performance of various echo-ranging sonars from the point of view of equipment figure of merit and range performance. In this paper, it is shown that the prediction method gives results which compare favorably with operational range performance data. Studies E, F, and G present three operational applications of Project AMOS results to surface vessel, echo-ranging sonar performance prediction problems.[20] In these studies the expected performance of echo-ranging sonars under various environmental and operational conditions is discussed.

Study H contains a very useful and interesting approach to the problem of ray tracing and field intensity computations. In Studies I and J these methods are applied especially to the energy propagated through the deep ocean by way of the SOFAR channel to focusing regions. A more detailed application of this theory is made to the data obtained in connection with the Project AMOS low-frequency broad-band noisemaker runs. It is shown that the quantitative features of the data can be explained by the theory.

---

[20] The concepts of "probability of detection" and "lateral range curves" are discussed in detail in USL Report No. 147.

SUMMARY REPORT OF AMOS CRUISE TWELVE[21]

The Oceanographic Survey Unit for Cruise TWELVE consisted of the USS SAN PABLO (AGS-30), CAPT W. D. Day (Commander Oceanographic Survey Unit); and the USS REHOBOTH (AGS-50), CAPT R. R. Snyder.

[21] The summary report of AMOS Cruise TWELVE was prepared by LT E. C. Iselin, Jr., Hydrographic Survey Officer at the Underwater Sound Laboratory. The operation order for this cruise appears in letter from the Hydrographer to ComSubLant, "Technical Instructions for AMOS Cruise TWELVE; forwarding of," ser. 09483, 31 December 1952 (CONFIDENTIAL). The measurements to be taken on this cruise were proposed in USL letter to the Hydrographer, "AMOS Cruise 12; schedule of," ser. 1170-056, 14 November 1952 (CONFIDENTIAL).

AMOS Cruise TWELVE was planned primarily from the standpoint of obtaining the maximum amount of acoustic data supported by the necessary oceanographic and seismic operations. The following measurements were proposed by the Laboratory:

a. 27 Acoustic Event 1
b. 27 Acoustic Event 8A

12

c. 27 Acoustic Event 3

d. 27 Acoustic Event 6

e. 5 Special Acoustic Events

f. 2 Acoustic Event 8C

The following itinerary was set for this cruise:

Date (1953)	Arrival-Departure	Place
26 January	Departure	Norfolk, Va.
30 January	Arrival	New London, Conn.
7 February	Departure	New London, Conn.
23 February	Arrival	Bermuda
27 February	Departure	Bermuda
13 March	Arrival	Trinidad, B.W.I.
17 March	Departure	Trinidad, B.W.I.
26 March	Arrival	San Juan, P. R.
30 March	Departure	San Juan, P. R.
10 April	Arrival	Nassau
13 April	Departure	Nassau
23 April	Arrival	Philadelphia, Pa.

The total cruise time was 88 days. Of this time 64 were spent at sea.

The following Laboratory personnel participated in AMOS Cruise TWELVE:

USS SAN PABLO	USS REHOBOTH
LT E. C. Iselin, Jr.	ENS B. B. Nichols
ENS B. B. Halleck	Mr. W. H. Thorp
Mr. H. F. Bernier	Mr. L. C. Maples
	Mr. F. G. Weigle
	Mr. O. P. Dickson
	Mr. S. F. Niedzwecki

ENS Nichols transferred from REHOBOTH to SAN PABLO in Trinidad. Mr. H. Johnson, of WHOI, was embarked in REHOBOTH during the Norfolk-to-New London and Bermuda-to-Trinidad legs.

EVENT 1: FOUR-FREQUENCY TRANSMISSION-LOSS MEASUREMENTS

Twenty-two Event 1 stations were made on AMOS Cruise TWELVE. Since the multi-element line hydrophone was not available, an alternate operating procedure was developed. Briefly stated, pulses were transmitted while the transducers were raised from 500 feet to 20 feet. Receiving trans- ducers were stationed at 20, 50, 100, 250, and 500 feet with one transmitting run for each receiving depth. Standard ranges for Event 1 were 3000, 8000, 12,000, 18,000, and 24,000 yards. When bathythermograph conditions were such that no transmissions were to be expected at 24,000 yards, an additional range of 5000 yards was taken.

EVENTS 4 AND 5: VERTICAL REVERBERATION MEASUREMENTS (12 KC) AND DEEP SCATTERING LAYER MEASUREMENTS

No Event 4 and Event 5 data were obtained. As a result of heavy pounding of the SAN PABLO during the first and second leg, the AN/UQN-1 fathometer transducer was damaged. A replacement was installed in Bermuda, but high-quality reception was not obtainable.

EVENT 6: VERTICAL TRANSMISSION AND SCATTERING LAYER MEASUREMENTS (8, 16, AND 24 KC)

No Event 6 data were obtained because of fathometer transducer difficulties on the REHOBOTH. At first these difficulties were attributed to crystal failure, but later they were found to be caused by broken crystal leads.

13

EVENTS 8A AND 8B: LOW-FREQUENCY PROPAGATION MEASUREMENTS

A total of 25 Event 8 type measurements were made. Subdivided by types they were:

Event 8A	Event 8B
11 with Mk 4	4 with bombs only
3 partial runs with Mk 4	
7 runs with bombs only	

No complete siren runs were made. Repeated mechanical casualty to the siren and pump overheating problems precluded its effective use on AMOS Cruise TWELVE. One short run using the Mk 6 was made to obtain the "signature" of the device as a sound source.

The schedule included the six special events described below. Detailed reports of these events, complete with track charts and logs, are being prepared for distribution.

ABLE (Site 1): A combination of unsuitable weather and lack of coordination between the aircraft and Office of Naval Research resulted in failure to this event.

BAKER: Special Event BAKER started at 201244Z February, 120 miles northwest of Bermuda. During the course of the circular run and the final radial run into Bermuda, 360 bombs were fired. Except for time out of commission, the Mk 4 was operated intermittently according to schedule. The final bomb of Phase I was fired at 230538Z February. The depth of detonation of the SOFAR shots is doubtful. The detonators used were observed to give erratic results and caused detonation to vary from premature to none at all. Phase II started at 282015Z February. A total of 147 bombs were fired. The event ended at 020630Z March.

CHARLIE: This event was executed by the seismic personnel and will be reported by them. However, cursory analysis of the data shows no evidence supporting the existence of Echo Bank.

DOG: This event started at 222204Z March. One hundred and two bombs were fired. The Mk 4 operated one hour on, one hour off. No Mk 4 casualties were experienced. Phase I ended at 240100Z March. Phase II started at 301707Z March. The two runs (070° and 304°) were run in accordance with the planned schedule. Sixty bombs were dropped on each run. On the 400-mile run on bearing 007°, 260 bombs were fired. The event ended at 010043Z April.

EASY: Special Event EASY started at 081304Z April. Forty-three bombs were fired. The Mk 4 was operated according to schedule. Phase I ended at 091219Z April and Phase II started at 132212Z April. Seventy-eight bombs were fired. The Mk 4 operated without failure. The event ended at 142345Z. Upon completion of this event the signature run of the Mk 6 was made.

ABLE: (Site 2): To utilize time more economically it was decided to abandon the site of the first Event 8C. It was planned to conduct Special Event ABLE and Event 8C at Site 2. Event ABLE was almost completed when heavy weather caused abandonment of the site.

The following major material casualties and deficiencies were noted:

a. In order to keep the Mk 4 operative, continuing maintenance was required. Four diaphragms were used.

b. The Mk 6 can not be towed at speeds over 5 knots. It was not used except for the one signature run.

14

EVENTS 8A AND 8B: LOW-FREQUENCY PROPAGATION MEASUREMENTS

A total of 25 Event 8 type measurements were made. Subdivided by types they were:

Event 8A	Event 8B
11 with Mk 4	4 with bombs only
3 partial runs with Mk 4	
7 runs with bombs only	

No complete siren runs were made. Repeated mechanical casualty to the siren and pump overheating problems precluded its effective use on AMOS Cruise TWELVE. One short run using the Mk 6 was made to obtain the "signature" of the device as a sound source.

The schedule included the six special events described below. Detailed reports of these events, complete with track charts and logs, are being prepared for distribution.

ABLE (Site 1): A combination of unsuitable weather and lack of coordination between the aircraft and Office of Naval Research resulted in failure to this event.

BAKER: Special Event BAKER started at 201244Z February, 120 miles northwest of Bermuda. During the course of the circular run and the final radial run into Bermuda, 360 bombs were fired. Except for time out of commission, the Mk 4 was operated intermittently according to schedule. The final bomb of Phase I was fired at 230538Z February. The depth of detonation of the SOFAR shots is doubtful. The detonators used were observed to give erratic results and caused detonation to vary from premature to none at all. Phase II started at 282015Z February. A total of 147 bombs were fired. The event ended at 020630Z March.

CHARLIE: This event was executed by the seismic personnel and will be reported by them. However, cursory analysis of the data shows no evidence supporting the existence of Echo Bank.

DOG: This event started at 222204Z March. One hundred and two bombs were fired. The Mk 4 operated one hour on, one hour off. No Mk 4 casualties were experienced. Phase I ended at 240100Z March. Phase II started at 301707Z March. The two runs (070° and 304°) were run in accordance with the planned schedule. Sixty bombs were dropped on each run. On the 400-mile run on bearing 007°, 260 bombs were fired. The event ended at 010043Z April.

EASY: Special Event EASY started at 081304Z April. Forty-three bombs were fired. The Mk 4 was operated according to schedule. Phase I ended at 091219Z April and Phase II started at 132212Z April. Seventy-eight bombs were fired. The Mk 4 operated without failure. The event ended at 142345Z. Upon completion of this event the signature run of the Mk 6 was made.

ABLE: (Site 2): To utilize time more economically it was decided to abandon the site of the first Event 8C. It was planned to conduct Special Event ABLE and Event 8C at Site 2. Event ABLE was almost completed when heavy weather caused abandonment of the site.

The following major material casualties and deficiencies were noted:

a. In order to keep the Mk 4 operative, continuing maintenance was required. Four diaphragms were used.

b. The Mk 6 can not be towed at speeds over 5 knots. It was not used except for the one signature run.

14

STUDY A

SOUND TRANSMISSION AT FREQUENCIES BETWEEN 2 AND 25 KILOCYCLES PER SECOND[1]

by

H. W. Marsh and M. Schulkin

INTRODUCTION

An analysis of AMOS transmission data in the 2- to 25-kc frequency region has been completed. The results of this analysis are presented in this

memorandum. A comprehensive discussion of these results, including comparison with other existing data, and recommendations for applications will be given in a forthcoming Laboratory report.

METHOD OF ANALYSIS

A definite model of the ocean as a transmitting medium has been used in carrying out this analysis. Reference to Fig. 1 will show that there are
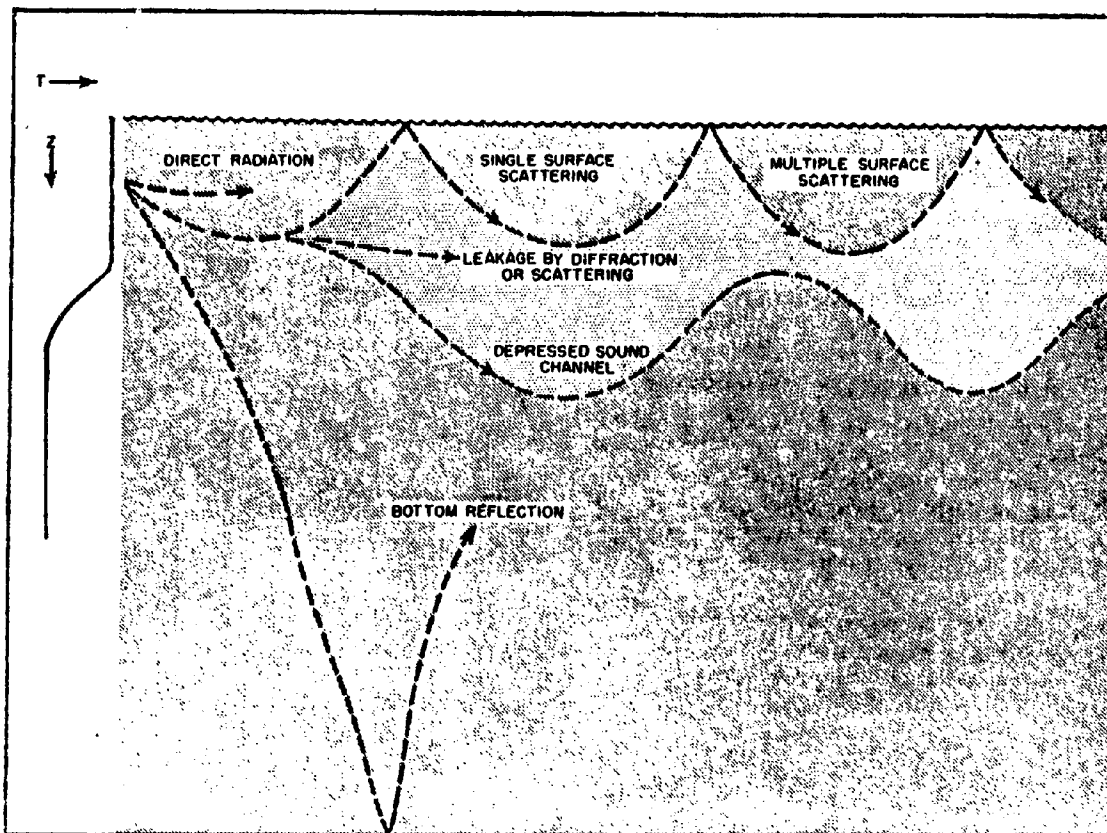
Fig. 1 - Modes of Sound Transmission

15

several modes of propagation which determine transmission conditions under any given set of circumstances. Sometimes the different modes are of comparable importance and must be combined in order to estimate the net sound field. At other times the sound field is dominated by a single mode of transmission.

In the present analysis an effort has been made to study the various modes separately. This can be done to a great degree by a proper selection of data according to the different oceanographic factors and according to the geometry and acoustic frequency associated with the data. Those factors which have been determined to be of importance are:

   a. Depth of isothermal (surface) layer
   b. Sea state (wind force)
   c. Depth of axis of depressed sound channel
   d. Depth of ocean bottom
   e. Water temperature
   f. Range
   g. Depth of source
   h. Depth of receiver
   i. Acoustic frequency

By scaling and by certain laws of combination, it is possible to reduce substantially the number of parameters required to characterize any particular mode. Thus, it is possible to prepare a limited set of charts or tables which, together with a small amount of computation, can be used to determine transmission loss under any prescribed condition lying within the framework of the analysis.

THE BASIC MODES OF TRANSMISSION

Transmission via modes associated with the surface isothermal layer and various orders of surface scattering (including negative surface gradient) may be scaled to layer depth and described in terms of a few simple formulas, which are listed after the definitions below. Source and receiver depths may be used interchangeably in applying these formulas. However, the conditions applying to the formulas are stated only for $Z_0 \leq Z$.

The following definitions and symbols will be used:

Basic Variables

Surface Isothermal Layer Depth (ft)	L
Sea State	S

Depth of Axis of Depressed Sound Channel (ft) D
Depth of Ocean Bottom (fm) B
Water Temperature (deg. F.) T
Range (kyd) R
Depth of Source (ft) Z_0
Depth of Receiver (ft) Z
Acoustic Frequency (kc) f
Relaxation Frequency (kc) f_T
Transmission Loss (db) N_w
Spreading Loss (db) $\begin{cases} 10 \log R, \\ 20 \log R \text{ (Fig. 2)} \end{cases}$
Absorption Coefficient (db/kyd) a (Fig. 3)
Scattering Coefficient (db/kyd) a_s (Fig. 4)
First Depth-Loss Factor G (Fig. 5)
Second Depth-Loss Factor H (Fig. 6)
Bottom Loss (db) N_B (Fig. 7)

Scaled Variables

$$r = R/\sqrt{L},$$

$$x_0 = \sqrt{Z_0}/\sqrt{L},$$

$$x = \sqrt{Z}/\sqrt{L},$$

$$r_1 = \frac{1}{4}\left[2 - x - x_0\right]; \quad x \leq 1, \ x_0 \leq 1;$$

$$r_1 = \frac{1}{4}\left[1 - x_0\right] + \frac{1}{5}\sqrt{x^2 - 1}; \quad x \geq 1, \ x_0 \leq 1;$$
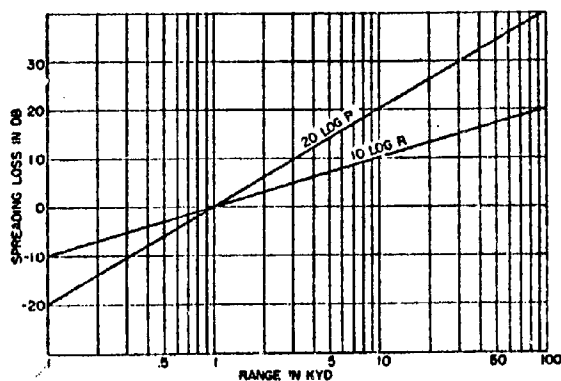
$$r_1 = \frac{\sqrt{x_0^2 - 1} + \sqrt{x^2 - 1}}{5}; \quad x, \ x_0 \geq 1.$$
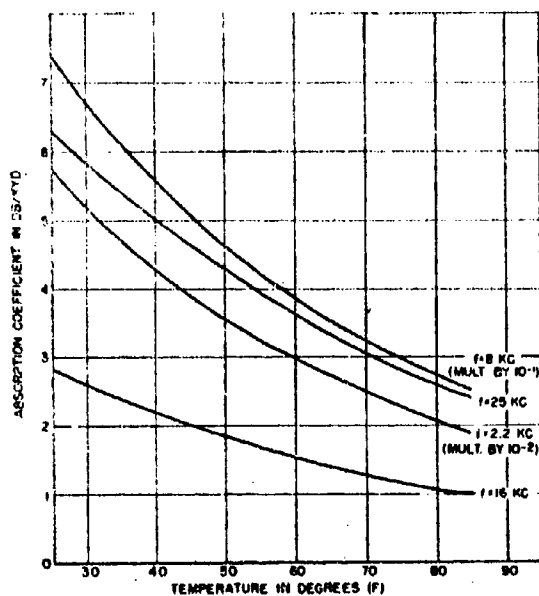

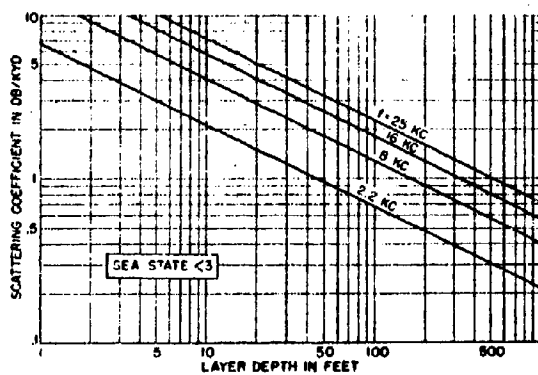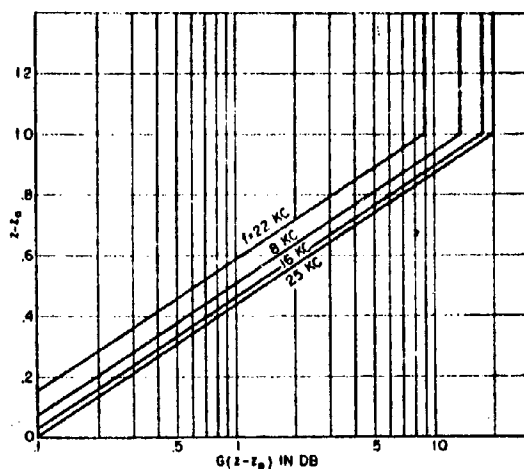Fig. 2 - Spreading Loss (db)

16

Fig. 3 - Absorption Coefficient (db/kyd)

Fig. 5 - First Depth-Loss Factor (db)
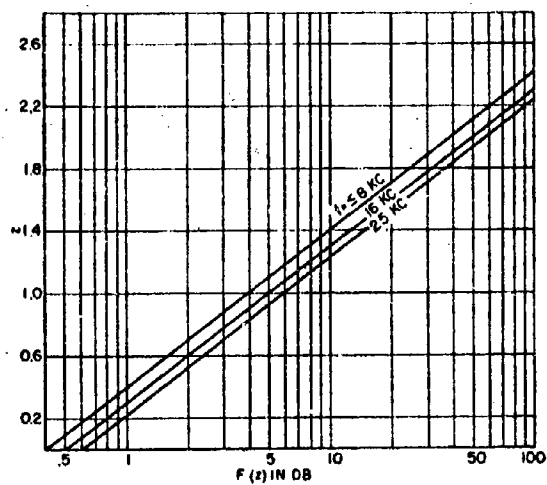
Fig. 6 - Chart for Computing Second Depth-Loss Factor, $H(z, z_0)$

Fig. 4 - Scattering Attenuation Coefficient (db/kyd)
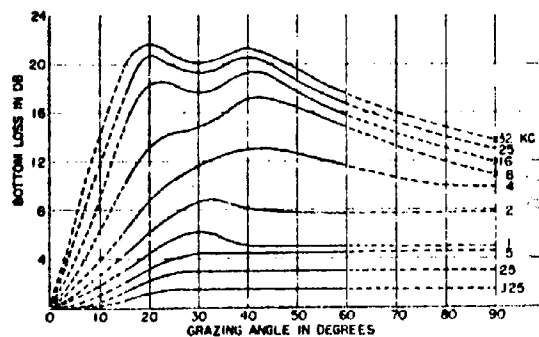

Fig. 7 - Bottom Loss vs. Grazing Angle

17

The propagation-loss formulas for the various modes of propagation are the following:

Direct Radiation Zone (Zone I), $0 \leq r \leq r_1$

When both ends of the transmission path lie within or at the bottom of the surface layer, the following formula applies:

$$N_w = 20 \log R + aR + G (z - z_o) \frac{r}{r_1} + 60 . \quad (1)$$

At all other times use the smaller of the two transmission losses computed by Formula (1) and the following:

$$N_w = 20 \log R + aR$$
$$+ [25 - \sqrt{|Z - L|} - \sqrt{|Z_o - L|} + 5R] \left(\frac{f}{25}\right)^{1/3}$$
$$+ 60 . \quad (2)$$

The quantity within the parentheses, multiplying the frequency term, is taken as zero when it is not positive.

Zone of First-Order Surface Reflection and Shadow Zone (Zone II)

Two propagation modes occur in Zone II:

Energy has been reflected at least once at the surface. The area covered is $z_o \leq 1, r_1 \leq r \leq r_1 + \frac{1}{2}$. Then,

$$N_w = 20 \log R + aR + 2 (r - r_1) H (z, z_o)$$
$$+ [1 - 2 (r - r_1)] G (z - z_o) + 60 . \quad (3)$$

The shadow zone beyond the limiting ray is delineated by

$$z_o \geq 1, z \geq 1, r_1 \leq r \leq r_1 + \frac{1}{2} .$$

For Zone II use Formula (3) or Formula (2), whichever yields the smaller propagation loss.

Zone of Second- or Higher-Order Surface Reflection (Zone III)

Energy has been reflected at least twice at the surface. It covers the area $z_o \leq 1, r_1 + \frac{1}{2} \leq r$. Then,

$$N_w = 10 \log R + (a + a_s) R + H (z, z_o)$$
$$- a_s \sqrt{L} (r_1 + \frac{1}{2})$$
$$+ 10 \log [\sqrt{L} (r_1 + \frac{1}{2})] + 60 . \quad (4)$$

The shadow zone beyond the limiting ray is delineated by

$$z_o \geq 1, z \geq 1, r_1 + \frac{1}{2} \leq r .$$

For Zone III use Formula (4) or Formula (2), whichever yields the smaller propagation loss.

Transmission Via Depressed Sound Channel

For this mode, the depths of the source and the receiver are referred to the axis of the channel as the origin, and the channel half-width, equivalent to the layer depth of a surface isothermal layer, is taken to be one-half the depth of the axis. Thus,

$$N_w = 20 \log R + aR$$
$$+ H \left(\sqrt{\frac{2 |Z - D|}{D}} , \sqrt{\frac{2 |Z_o - D|}{D}} \right) + 60 . \quad (5)$$

Transmission Via Bottom Reflection

Transmission takes place by one bottom reflection:

$$N_w = 20 \log R + aR + N_B + 60 , \quad (6)$$

where R is the slant range from the source to the bottom to the receiver for specular reflection and N_B is the bottom loss for the grazing angle at the point of reflection and is given in Fig. 7.

ANALYSIS OF DISPERSIONS

The probable errors of the propagation loss estimated by this method are given below:

18

Probable Errors of Propagation-Loss Predictions (AMOS) (±db)

Frequency (kc)	2.2	8	16	25
Mode of Transmission (Formulas 2 and 5)	6.5	5	6.5	9
Mode of Transmission (Formulas 1, 3, and 4)	4	3	4.5	5
Reciprocal Difference	3.5	2.5	1.5	3.0

These errors result partly from the inadequacies of the method, from basic fluctuations which can not be predicted, and from errors of measurement. In order to estimate the fluctuations, a study has been made of the sound fields measured under identical conditions but with the source and the receiver interchanged. The difference between the two measurements is referred to as a reciprocal difference. Except for that mode of transmission associated with Formulas (2) and (5), the error of estimation is approximately 1-1/2 db greater than the mean reciprocal difference. The probable er-

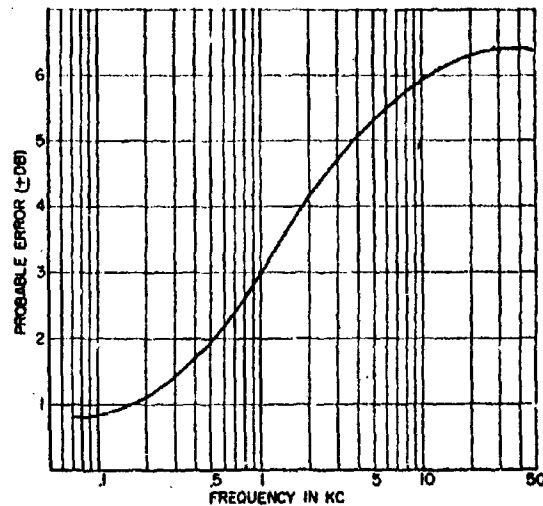rors associated with the bottom reflection data (Fig. 7) are given in Fig. 8.

Fig. 8 - Probable Error in Bottom Loss vs. Frequency

ASSOCIATED COMPUTATIONAL FACTORS FOR PROPAGATION LOSS

In order to compute the individual terms of the propagation modes, the following formulas are required:

Absorption Coefficient (db/kyd) (see Fig. 3)

$$a = \frac{A f^2 f_T}{f^2 + f_T^2} + \frac{B f^2}{f_T}, \tag{7}$$

where

$$A = 0.651, \quad B = 0.0269,$$

$$f_T = 1.23 \times 10^6 - [2100/(T + 459.6)]$$

$$= 1.23 \times 10^6 \times e^{-4830/(T + 459.6)},$$

and then

$$A/B = 24.2; \quad f_{50} = 93.$$

For low frequencies,

$$a \sim \frac{0.678 \, f^2}{f_T},$$

and

$$a_0 \sim 0.0073 \, f^2 \text{ for } T = 50° F.$$

Scattering Attenuation Coefficient (db/kyd) (see Fig. 4)

$$a_s = 4.5 \left(\frac{f}{L}\right)^{1/2}, \quad S < 3$$

$$= 9 \left(\frac{f}{L}\right)^{1/2}, \quad S \geq 3.$$

First Depth-Loss Factor (db) (see Fig. 5)

$$G(z - z_0) = 0.1 \times 10^{2.3(z - z_0)} (f/25)^{1/3}, (z - z_0) \leq 1$$

$$= 20 \, (f/25)^{1/3}, (z - z_0) \geq 1.$$

Second Depth-Loss Factor (db) (computed from Fig. 6)

$$H(z, z_0) = F(z - z_0) + F(z) + F(z_0),$$

where

$$F(z) = 0.4 \times 10^z \left(\frac{f}{8}\right)^{1/3}, \quad f \geq 8;$$

$$= 0.4 \times 10^z, \quad f \leq 8.$$

19-20

STUDY B

CONTOURS OF TRANSMISSION LOSS FOR
STANDARD CONDITIONS AND CORRECTION CHARTS[1]

by

M. R. Powers, K. R. Dickson, and L. P. Onyx

INTRODUCTION

Contours of standard transmission loss, N_{wo}, have been plotted for ten frequencies and three projector depths, for a standard temperature (50° F.) and a standard layer depth (100 feet). Correction charts have been plotted for each frequency for the correction required because of changes in layer depth, temperature, and sea state. Values of the absorption coefficient, a, for various temperatures are also included. The corrections are to be added to the standard transmission loss. The loss contours and correction charts for each frequency have been grouped together for ready reference.

METHOD OF COMPUTATION

The values of the transmission loss first were computed from Formulas (1), (3), and (4) of Study A. In all the computations a layer depth of 100 feet, a temperature of 50° F., and a sea state of less than 3 were assumed. Computations were made for projector depths of 20, 50, and 100 feet, for frequencies of 2, 10, and 25 kc.[2] For each projector depth and frequency, the standard transmission loss was computed at seven receiver depths and eight ranges. These values were used to plot contours of constant loss. Examples of such contours are given in Figs. 1A through 1C, 3A through 3C, and 5A through 5C.

A plot of transmission loss for Formula (2) of Study A was also made for each frequency. The

loss was computed as a function of Σ, where

$$\Sigma = \sqrt{|Z - L|} + \sqrt{|Z_0 - L|} .$$

The curves were plotted for constant range, R, between 0.5 and 25 kyd, for values of Σ from 0 to 140. These curves should be used when they give a smaller loss value than the value computed from Formulas (1), (3), and (4) of Study A but can not be used when both the projector and the receiver are above the layer. Examples of these computations are given in Figs. 1D, 3D, and 5D.

The layer-depth correction was computed from the formula:

$$\Delta_L = 10 \log \frac{L}{L_0} - a_0 R \left(\frac{\sqrt{L_0}}{\sqrt{L}} - 1 \right),$$

where

   L = layer depth (ft),

   L_0 = standard layer depth = 100 ft,

   a_0 = absorption coefficient (db/kyd) at
       $T = 50°$ F., and

   R = range (kyd).

This formula was evaluated for twelve values of L between 9 and 1024 feet. Curves were plotted for Δ_L versus R, for constant L. The contours of constant Δ_L (see Figs. 2, 4, and 6) were plotted by interpolating in these curves. This correction applies to Formulas (1), (3), and (4) of Study A.

In order to find the transmission loss for a given R, Z, and Z_0, for a layer depth different from 100 ft, it is necessary to find the values of the scaled variables r, z, and z_0 by using the actual layer depth. The standard loss contours are entered with r, z, and z_0, and the value of N_{wo} is read. The correction term is found from the layer correction contours, where these curves are entered with R and L.

[1] This report, together with a complete set of working charts, appeared originally as USL Technical Memorandum No. 1110-101-54, 17 August 1954 (UNCLASSIFIED).

[2] The original computations were made at additional frequencies of 1, 5, 8, 12, 14, 20, and 31 kc. However, the computations for the 1-kc frequency are extrapolated from data at higher frequencies and thus are to be considered as estimates only.
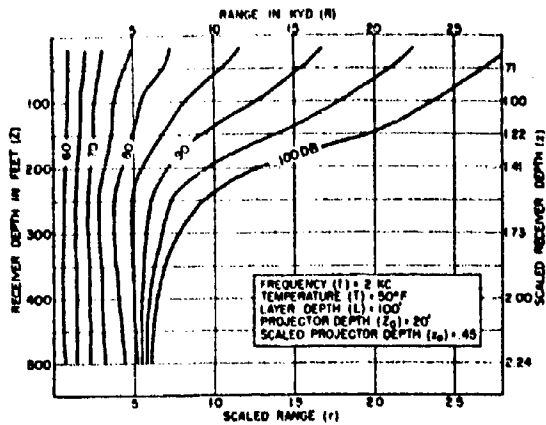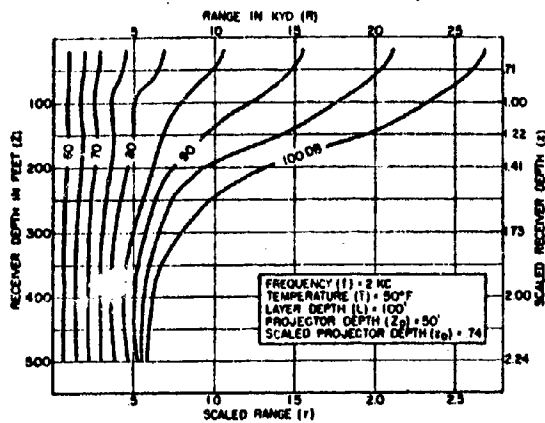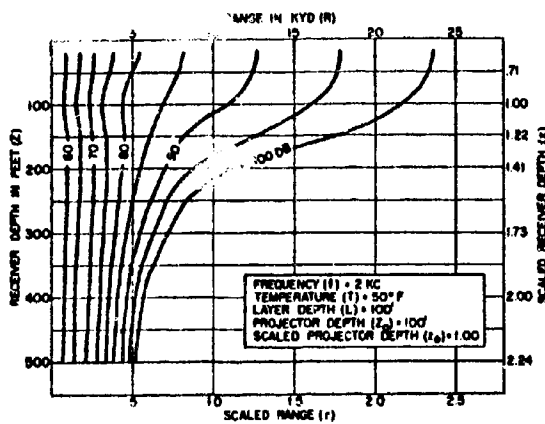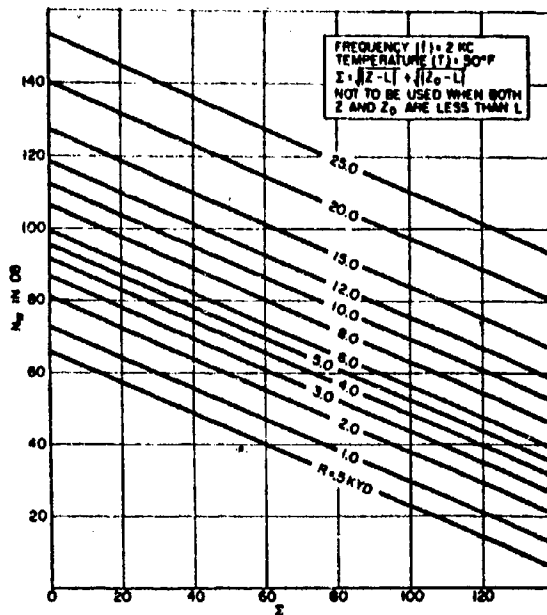
Fig. 1A

Fig. 1B

Fig. 1C

Fig. 1D

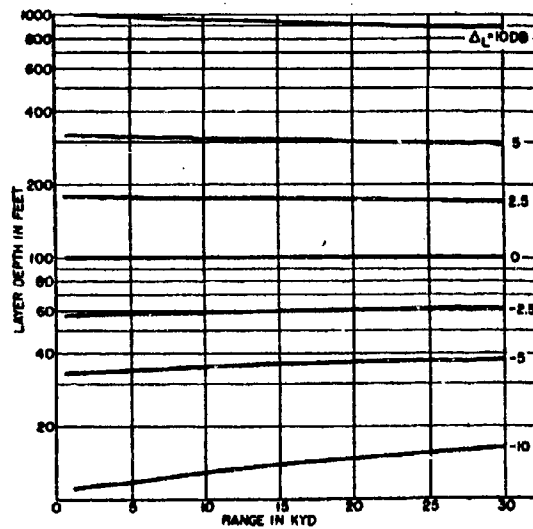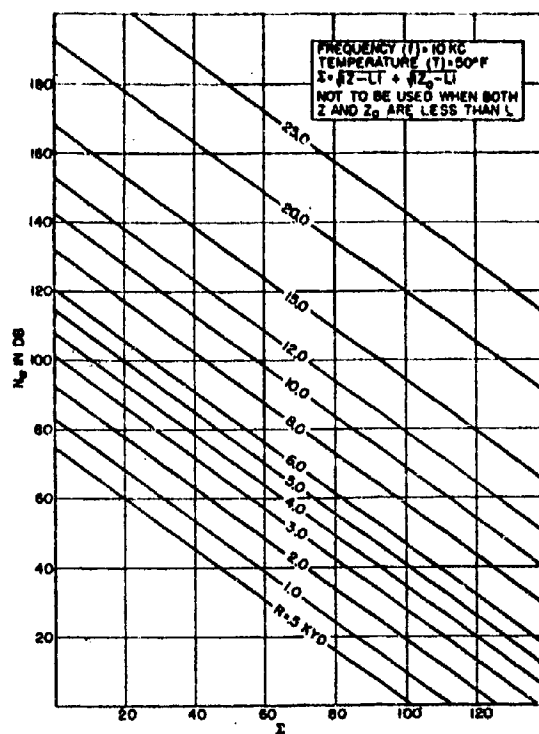Fig. 1 - Propagation-Loss Contours
(in db for 2-kc frequency)
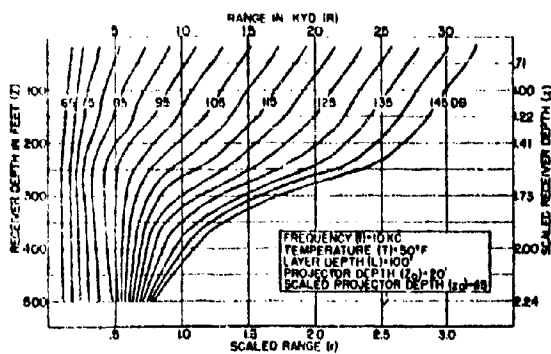

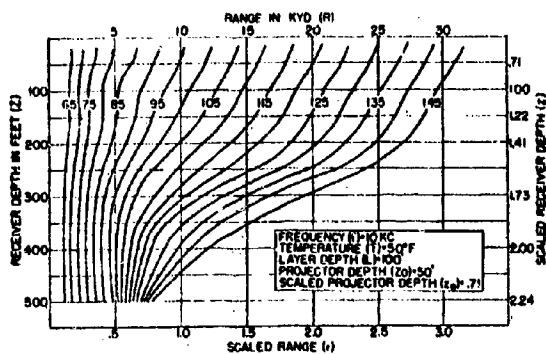Fig. 2 - Layer-Depth Correction Contours (2 kc)

Fig. 3A

Fig. 3B

Fig. 3C

Fig. 3D

Fig. 3 - Propagation-Loss Contours
(in db for 10-kc frequency)
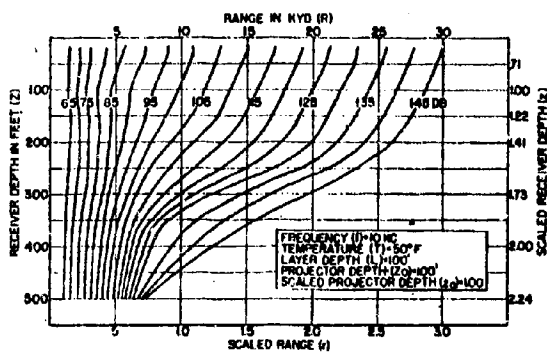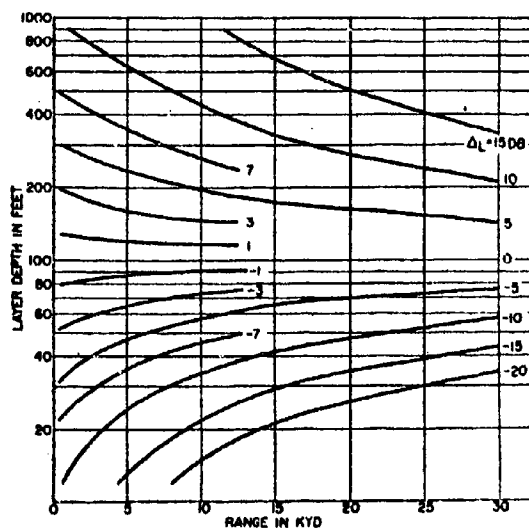
Fig. 4 - Layer-Depth Correction Contours (10 kc)

23

Fig. 5A

Fig. 5B

Fig. 5C

Fig. 5D

Fig. 5 - Propagation-Loss Contours
(in db for 25-kc frequency)

Fig. 6 - Layer-Depth Correction Contours (25 kc)

24
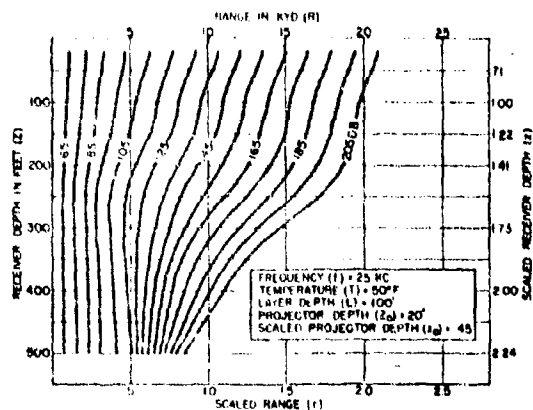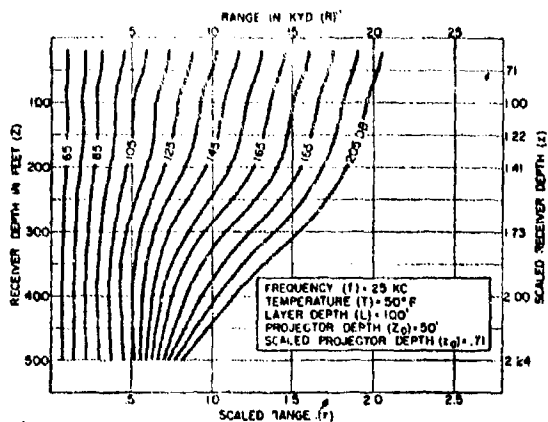
Fig. 7A - 2 kc

Fig. 7B - 10 kc
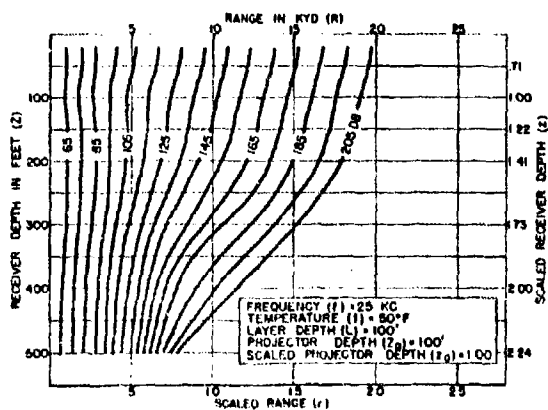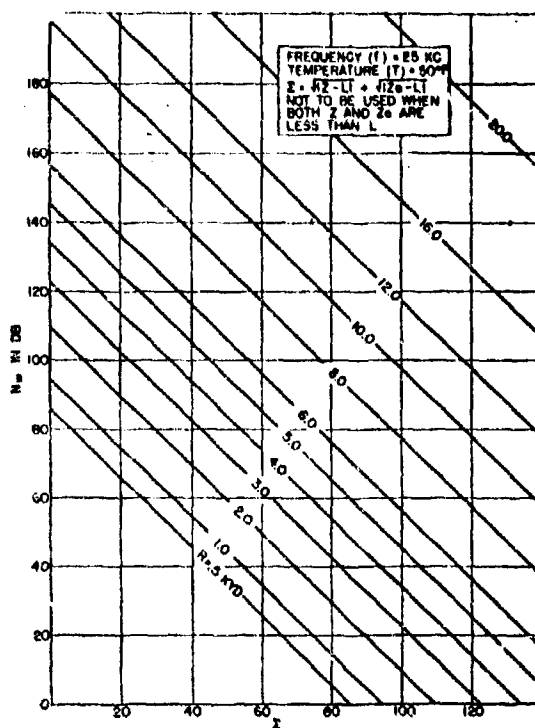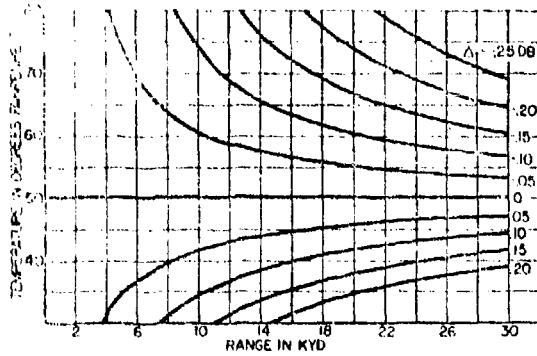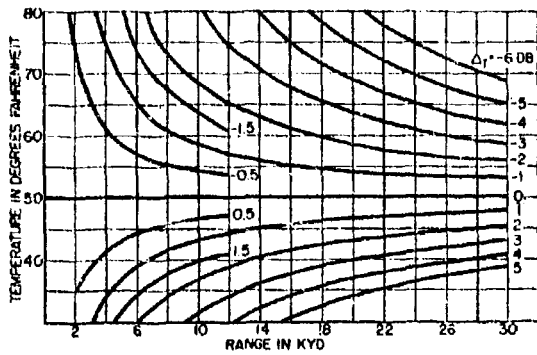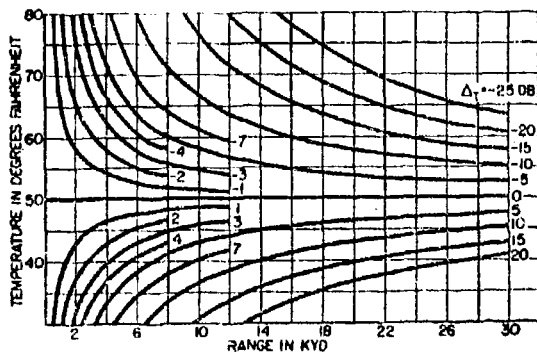

Fig. 7C - 25 kc

Fig. 7 - Temperature Correction Contours
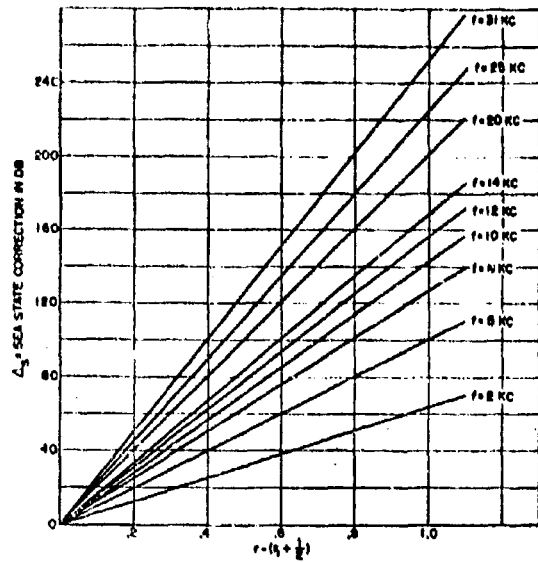(2 kc, 10 kc, and 25 kc)

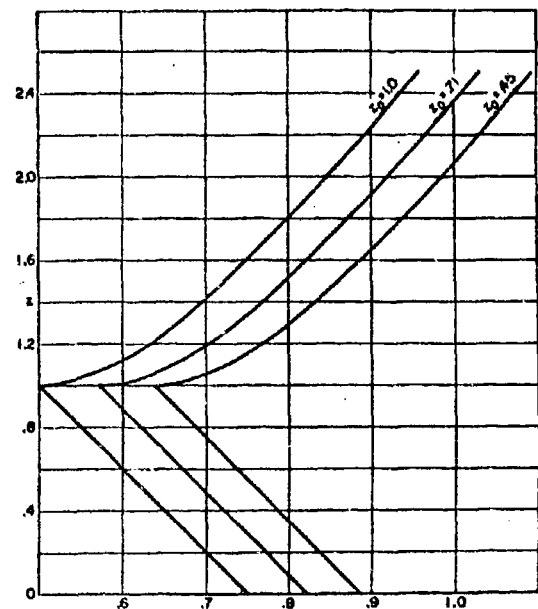Fig. 8 - Sea-State Correction (for Sea State 3 or Greater)

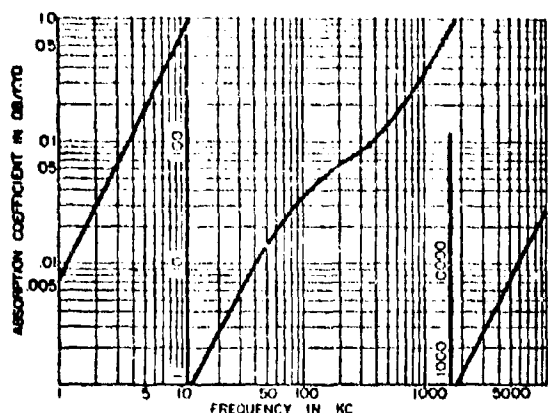Fig. 9 - Scaled Range in Propagation Zone III vs. Depth

Fig. 10 - Absorption Coefficient (in db/kyd) vs.
Frequency (in kc) for $T = 50°$ F.

The temperature correction contours were plotted
in a manner similar to that used for the layer cor-
rection:

$$\Delta_T = a_0 R\left(\frac{a}{a_0} - 1\right),$$

where

a   is evaluated at temperature $= T°$ F.,

a_0 is evaluated at standard temperature
    $= 50°$ F., and

R   is range (kyd).

The formula was evaluated for six values of T
between 30° and 90°, and the curves were plotted
for Δ_T versus R at a constant T. The contours of
constant Δ_T (see Figs. 7A, 7B, and 7C) were
plotted by interpolating in these curves. This cor-
rection applies to all propagation zones.

It should not be assumed that interpolation in
these correction charts will be accurate for an in-
terval smaller than one-half the interval between
contours. If greater accuracy is desired, the cor-
rection values should be found from the formulas
or from graphs for constant L or T. This is particu-
larly true for ranges of less than one kiloyard.

The sea-state correction

$$\Delta_s \sim 4.9 f^{1/2} \left[r - (r_1 + \tfrac{1}{2})\right]$$

has been plotted for each frequency (Fig. 8). This
is applicable only for the ranges $r \geq r_1 + \tfrac{1}{2}$, for
which Formula (4) of Study A applies. These ranges
may be determined by using Fig. 9 for the three
values of projector depth ($z_0 = 0.45$, 0.71, 1.00,
or $Z_0 = 20$, 50, 100 feet).

Figure 10 gives the values of a_0 for frequen-
cies from 1 to 10,000 kc, at $T = 50°$ F. The values
of $c = a/a_0$ are plotted for temperatures from 25°
to 80° F. and for frequencies from 1 to 10,000 kc
(Fig. 11).

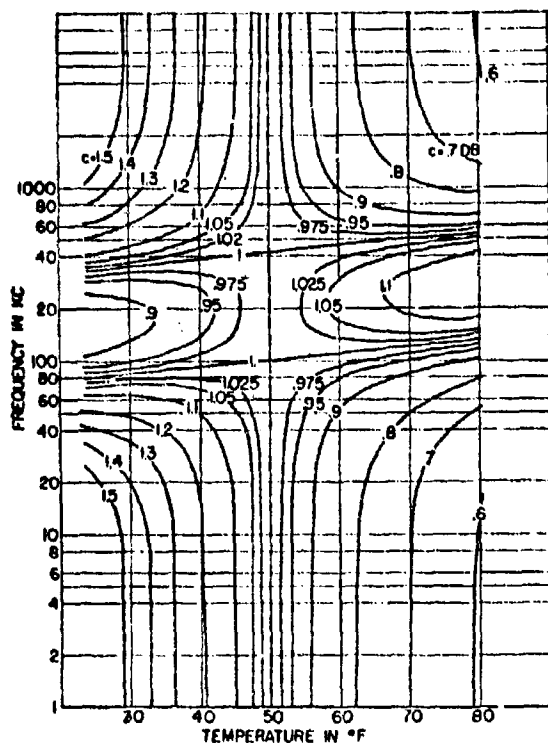

Fig. 11 - Temperature Dependence of Absorption
Coefficient Ratio ($c = a/a_0$)
(a_0 = Absorption Coefficient at 50° F.)

26

STUDY C

ERROR STUDY OF AMOS PROPAGATION-LOSS ANALYSIS

by

W. H. Thorp

An investigation was made of the magnitude of errors to be expected from the use of the analytical formulas given in Study A of this report for the estimation of propagation loss. This was done by working with a representative sample of the entire data file. This sample was obtained by selecting at random a single IBM card to represent each of the North Atlantic deep-water stations which were occupied between 1949 and 1953. Each card so selected contained the measured values of propagation loss for one or more of the four discrete acoustic frequencies (2, 2, 8, 16, and 25 kc) for a given range and projector-receiver depth pair. These data are listed in Table 1.

The mode of propagation which applied to each particular station card was determined from a consideration of the pertinent parameters as indicated in Study A. The corresponding values of propagation loss were then computed from the formulas of Study A. It should be noted that more than one propagation mode may apply under the transmission conditions; therefore, calculations using each applicable formula must be made and the result which indicates the least loss must be chosen. This, in effect, increases the numerical effort required by about 50%.

In Table 2 are presented the probable errors of the prediction method obtained by subtracting the computed values of propagation loss from the measured values for the indicated propagation modes for the 149 stations of Table 1. For the remaining nine stations, the prevailing propagation mode appeared to be by way of the ocean bottom.

The magnitude of the probable errors reflects some of the time variability of the ocean itself as a propagation medium. This effect was estimated in this study by considering the reciprocal nature of propagation over the same path with transmitting and receiving positions interchanged within a period of from 15 to 20 minutes for most of the stations in Table 1. The reciprocal differences referred to in Table 2 are the differences in measured propagation loss over the same path, but with receiver and projector positions interchanged. It may be seen that a sizable part of the probable error of estimation arises from the time variability introduced by the ocean. These errors appear to be independent of range over the ranges of the AMOS experiments (1 to 25 kyd).

It may be seen that the probable errors for the downward refraction mode of propagation appear to be larger than those associated with surface channel propagation. The errors associated with propagation by way of the bottom are treated separately in Study D.

Table 1

COMPARISON OF COMPUTED AND MEASURED AMOS PROPAGATION LOSSES

Cruise	Station	Layer Depth (ft)	Sea State	Surface Temperature (°F)	Projector Depth (ft)	Receiver Depth (ft)	Range (yd)	Propagation Formula[a]	2.2 kc N_w	2.2 kc N_{wo}	8 kc N_w	8 kc N_{wo}	16 kc N_w	16 kc N_{wo}	25 kc N_w	25 kc N_{wo}
2	1	30	1	74.1	15	320	800	(1)							71	65
	2	150	0	79.0	15	260	500	(2)							52	57
	3	100	1	76.6	15	40	3,000	(3)							91	79
	4	0	1	76.7	15	100	2,720	(2)							62	101
	5	25	4	75.0	15	120	1,950	(1)							82	89
	7	30	1	56.0	15	360	2,650	(1)							73	92
3	3	50	1	82.0	15	105	3,340	(3)							90	93
	6	0	1	81.5	15	360	4,200	(2)							91	107
	9	65	2	79.1	15	209	2,460	(1)							83	89
	12	60	1	78.4	15	445	2,950	(1)							95	90
	15	0	1	78.0	15	401	1,900	(2)							72	81
	18	25	1	79.0	15	495	1,480	(1)							64	74
	21	20	1	76.8	15	162	4,640	(6)							99	131
	24	100	1	74.1	15	480	2,950	(1)							80	89
	27	130	2	71.4	15	95	6,160	(3)							112	100
	32	0	1	76.5	15	500	3,950	(2)							97	102
	36	0	2	72.1	15	355	4,430	(2)							95	111
	39	75	2	68.9	15	20	3,300	(3)							81	82
	42	40	2	72.7	15	55	800	(1)							66	61
	45	75	1	67.6	15	505	3,150	(1)							105	92
	48	50	1	65.1	15	430	4,140	(1)							86	103
	50	75	1	63.0	15	20	4,800	(3)							87	93
	54	50	1	65.5	15	20	7,470	(4)							93	114
	57	20	1	60.8	15	245	2,260	(1)							74	91
	60	0	1	59.4	15	60	1,800	(2)							85	95
	63	120	3	53.4	15	20	3,320	(1)							83	84
	66	75	2	57.2	15	20	4,480	(3)							91	93
	69	100	2	65.5	15	40	3,080	(3)							78	81
	72	110	1	70.6	15	60	3,160	(3)							74	81
	75	0	0	74.2	15	440	5,280	(2)							111	116
	78	85	1	76.6	15	132	1,480	(1)							72	72
	81	75	2	74.5	15	500	2,440	(2)							86	84
	84	175	2	77.6	15	20	4,980	(3)							77	90
	87	85	1	80.0	15	90	2,880	(3)							86	82
	90	115	2	79.7	15	240	5,960	(3)							99	114
5	3	135	2	77.2	20	275	3,120	(1)			75	81	81	87	91	94
	4	135	1	80.0	300	300	5,250	(1)			92	91	100	96	113	100
	5	150	1	79.6	50	200	3,620	(3)			71	75	78	78	84	85
	6	150	1	77.3	20	175	3,180	(3)			74	74	74	78	85	84
	7	250	1	77.0	175	275	5,750	(3)			93	82				
	8	200	1	72.8	20	175	3,330	(3)			73	74	74	78	83	84
	9	325	3	68.0	50	200	3,100	(1)			73	72	82	75	83	81
	10	810	2	67.0	20	300	3,150	(1)			74	71	77	75	84	81
	11	50	3	43.4	300	300	7,850	(3)			80	105	96	122	118	148
	12	310	2	34.0	100	275	8,000	(3)			79	88	95	103	117	129
	13	490	2	56.0	20	50	8,000	(1)			82	82	94	92	111	111
	14	200	2	63.0	150	300	3,850	(3)					85	81	93	89
	15	430	2	63.0	20	20	15,960	(3)	102	91						
	16	100	4	61.0	20	150	15,300	(4)	105	102						
	18	650	1	54.0	100	300	2,720	(1)			69	70	75	74	79	80
	19	250	2	53.0	150	275	3,250	(3)			76	73	79	78	86	84
	20	125	2	70.8	20	450	1,270	(1)			62	65	63	68	77	71
	21	120	2	60.5	20	50	2,880	(3)			71	71	75	74	81	79

[a] From Study A.

(Continued)

Table 1 (Cont'd)

Cruise	Station	Layer Depth (ft)	Sea State	Surface Temperature (°F.)	Projector Depth (ft)	Receiver Depth (ft)	Range (yd)	Propagation Formula*	2.2 kc N_w	2.2 kc N_{wo}	8 kc N_w	8 kc N_{wo}	16 kc N_w	16 kc N_{wo}	25 kc N_w	25 kc N_{wo}
5	22	25	1	70.0	20	175	8,000	(6)			107	105	131	115		
	23	0	1	70.0	50	450	7,670	(2)			99	103	108	117	128	117
	24	30	1	71.0	250	350	5,300	(2)			81	89	84	97	98	110
	25	100	3	69.0	250	350	2,720	(2)			66	77	72	81	81	88
7	2	75	1	76.0	20	100	4,680	(3)			80	81	85	86	97	96
	3	125	2	79.9	200	400	7,900	(4)							133	119
	5	0	2	81.5	100	400	4,140	(2)							115	99
	6	175	2	81.0	20	20	7,950	(5)			80	81	94	88	126	101
	7	280	3	81.0	100	400	7,750	(5)			85	86	100	95	120	109
	8	260	2	75.5	50	100	4,000	(3)			61	74	78	77	79	94
8	1	480	3	68.0	50	150	5,220	(1)			79	77	81	82	82	92
	2	350	2	68.8	50	100	3,080	(1)			94	71	99	74	82	80
	3	390	2	69.2	450	450	12,000	(4)			106	78	102	89	137	108
	4	380	2	68.8	250	500	2,720	(1)			81	69	81	73	84	78
	7	440	2	67.1	150	450	8,100	(3)			91	85	97	94	111	110
	8	300	1	64.9	50	425	6,620	(3)			83	84	90	93	100	107
	9	0	1	61.4	20	200	1,520	(2)			65	73	65	78	65	83
	10	0	1	63.3	20	425	5,150	(2)			76	94	83	103	92	118
	11	0	1	60.4	20	100	8,770	(6)			79	95	87	112	106	133
	12	190	3	55.6	20	425	880	(2)			61	61	64	61	85	64
	13	260	2	60.1	50	350	5,800	(3)			87	82	91	90	106	103
	14	200	2	58.5	350	400	5,140	(3)			71	89	91	98	92	112
	15	340	2	57.0	50	250	2,860	(1)			70	71	69	75	77	82
	16	500	1	56.8	400	450	4,850	(3)			75	78	84	85		
	17	20	1	58.2	100	100	20,200	(6)			93	103				
	18	45	2	57.0	20	100	8,300	(4)			94	102	105	119	120	143
	19	300	3	53.0	20	450	7,800	(3)			76	73	91	107	107	127
	20	50	3	52.4	20	50	4,930	(4)			76	84	87	94	98	105
	21	100	2	52.4	150	400	17,400	(4)			94	104				
	22	65	2	56.0	20	50	18,150	(4)			103	113				
	23	120	2	65.9	20	100	12,200	(4)			95	92	113	112	133	149
	24	90	2	66.4	20	250	8,440	(3)			79	105	86	124	115	135
	25	110	3	66.8	100	200	17,900	(6)			98	113				
	26	40	1	66.1	20	50	17,900	(6)			99	113				
9	1	15	1	59.5	50	200	2,600	(2)			85	82	88	88	102	96
	3	30	1	55.0	50	100	2,960	(5)	64	75	73	76	75	81	89	89
	4	125	3	57.8	150	350	4,100	(3)			76	81	77	88	94	114
	5	100	5	51.0	450	450	7,700	(5)			84	88	101	101	119	121
	6	50	2	49.8	100	200	3,200	(5)			87	81	85	88	104	98
	7	40	1	50.8	50	100	8,220	(4)			106	75				
	8	60	1	50.5	150	250	4,600	(2)			96	93	103	103	134	118
	9	55	2	54.0	50	150	8,080	(6)	96	88	113	99				
	10	85	1	58.5	50	350	4,840	(3)			85	99	103	110	126	124
	11	75	1	66.0	95	260	1,930	(1)	80	68	79	69	82	83	100	76
	12	100	1	68.0	50	450	3,220	(1)							110	95
	13	100	1	70.0	50	200	3,260	(3)	93	73	97	75	99	80		
	14	40	2	68.0	50	150	3,500	(5)			93	87	104	94	129	104
	15	75	2	66.9	100	350	18,200	(5)	98	97						
	16	115	3	63.8	250	450	8,730	(4)			104	70				
	17	125	2	62.5	250	400	1,700	(1)			60	66	65	69	70	71
	18	80	2	59.0	100	350	8,400	(5)			113	94				
10	1	200	2	50.0	30	200	2,950	(3)			65	73	75	74	81	85
	2	1800	4	41.0	250	350	5,150	(1)			76	77	92	86	101	100

*From Study A.

(Continued)

29

Table I (Cont'd)

Cruise	Station	Layer Depth (ft)	Sea State	Surface Temperature (°F.)	Projector Depth (ft)	Receiver Depth (ft)	Range (yd)	Propagation Formula*	2.2 kc		8 kc		16 kc		25 kc	
									N_w	N_{wo}	N_w	N_{wo}	N_w	N_{wo}	N_w	N_{wo}
10	3	895	1	43.9	30	150	5,750	(1)			81	79	93	88	105	105
	4	1045	3	43.6	250	475	4,380	(1)			76	76	90	83	98	96
	5	1625	1	47.2	50	250	740	(1)			60	58	65	59	66	61
	6	1410	2	48.8	500	500	5,450	(1)			76	77	91	85	100	99
	7	1500	2	48.7	30	100	3,280	(1)			73	72	82	77	85	85
	8	1055	4	45.1	250	300	6,500	(1)			82	80	93	90	108	107
	9	300	2	37.7	100	150	3,320	(3)	68	71	74	73	94	90	95	88
	10	330	3	43.1	50	475	4,730	(1)	62	77	78	81	70	65	107	103
	11	650	3	47.3	50	150	1,340	(1)	65	63	61	63			69	69
	13	580	4	53.3	50	100	2,710	(1)	69	69					83	80
	15	55	1	59.1	250	250	3,800	(5)	72	81	84	83	76	90	84	100
	16	200	2	58.3	30	500	4,380	(3)	67	73	79	75	86	80	100	90
	17	65	2	59.9	30	50	1,850	(3)	69	76	77	77	83	83	96	92
	18	165	2	40.1	400	500	3,200	(3)			75	75	87	81	92	90
11	1	0	1	52.5	50	500	1,020	(2)			56	61	61	62	83	65
	2	75	2	47.5	150	250	2,760	(3)			73	79	79	86	89	95
	3	70	2	44.3	100	250	4,200	(5)	84	79					114	102
	4	60	2	46.2	250	475	5,290	(5)	73	81	71	83	81	93	99	106
	5	65	1	49.0	150	500	2,660	(2)	60	73	70	76	73	80	81	89
	6	0	1	50.4	250	475	4,740	(2)	71	79	74	84	79	91	90	103
	7	20	1	50.8	50	450	5,310	(2)			90	93	94	106	113	123
	8	15	1	50.0	20	475	5,890	(6)	85	85	96	95	110	110	134	131
	9	0	1	50.0	150	350	3,100	(2)	80	75	79	78	89	83	97	93
	10	0	2	44.5	100	475	5,530	(2)	85	85					118	122
	11	0	1	49.1	20	250	8,180	(6)	95	89	104	103				
	12	25	1	37.0	50	400	7,400	(6)	107	87	108	98	110	115	141	142
	13	0	1	39.0	200	500	5,540	(2)	89	83	87	89	101	101	120	119
	14	0	1	39.2	100	475	2,840	(2)	67	73	74	76	81	81	92	91
	15	40	2	52.0	20	250	18,000	(6)	95	93	107	108				
	16	50	1	52.5	250	350	5,600	(2)	81	85	93	93	105	103	120	119
	17	85	3	50.7	50	350	18,200	(6)	101	94	113	109				
	18	90	1	58.8	150	500	2,550	(2)	82	73	84	76	84	70	112	87
	21	50	2	67.3	100	300	3,120	(2)	83	78	91	83	100	89		
12	2	255	2	42.0	20	500	3,020	(1)							92	94
	4	900	3	63.2	103	253	8,310	(1)	81	80	75	83	104	93	117	110
	5	800	3	64.8	30	478	8,200	(3)	78	80	82	83	88	92	107	109
	6	50	2	71.9	20	500	5,480	(6)			89	105	99	133		
	7	0	2	78.5	20	299	8,840	(6)			94	109				
	8	360	3	75.2	20	251	8,760	(3)			94	84	108	93	93	109
	9	280	5	76.0	101	251	12,460	(4)			96	94				
	10	270	2	76.1	404	500	3,680	(3)	67	75	76	76	85	80	97	86
	11	120	3	77.7	98	251	3,080	(3)			75	73	81	77	86	82
	12	0	2	80.5	48	50	17,600	(6)	72	91	90	107				
	13	120	3	78.9	248	448	3,090	(3)	65	75	77	77	81	82	89	87
	14	30	2	79.2	20	52	8,420	(4)			81	99			101	133
	15	100	2	77.3	20	20	7,720	(3)	61	81	75	82	88	90	114	103
	16	135	1	71.2	20	50	3,500	(3)	51	71					77	83
	17	30	3	77.5	50	102	7,680	(4)	76	81						
	18	0	2	74.2	100	475	3,560	(2)	82	73	59	80	62	84	74	92
	19	0	2	75.5	20	51	18,140	(6)	81	96	96	115				
	20	100	2	71.0	441	500	7,860	(5)	75	85			93	97	123	112
	21	150	2	67.0	202	250	7,960	(3)					72	109		
	22	180	2	67.0	249	471	5,110	(5)	87	87	95	89	107	100	134	117

*From Study A.

30

Table 2

PROBABLE ERRORS OF
PROPAGATION-LOSS PREDICTIONS
(AMOS) (±db)

	2.2 kc	8 kc	16 kc	25 kc
Mode of Transmission (Formulas 2 and 5, Study A)	6.5	5.0	6.5	9.0
Mode of Transmission (Formulas 1, 3, and 4, Study A)	4.0	3.0	4.5	5.0
Reciprocal Differences	3.5	2.5	1.5	3.0

STUDY D

TRANSMISSION BY WAY OF THE BOTTOM

by

M. Schulkin and W. H. Thorp

INTRODUCTION

The deep-water bottom-reflection data available as of January 1954 have been assembled in a form which is suitable for use in sonar range predictions. No attempt is made to explain the data; rather, the data are described in terms of a model. The model used is that of propagation by way of the specular path, including an empirical loss at the bottom. At grazing angles approaching 0°, the behavior of the Rayleigh reflection coefficient is assumed. At perpendicular incidence, scattering coefficients deduced from AMOS vertical sounding measurements at 2, 8, and 34 kc were used.

The most extensive sources of bottom-reflection data in deep water for the 2- to 25-kc frequency range are AMOS Cruises NINE, ELEVEN, and TWELVE. Cruises NINE and ELEVEN were notable for their shallow surface sound channels and low, direct acoustic fields at short ranges. As continuous-wave sources were used on these two cruises, the sound energy could arrive by various paths, and some discretion had to be used in selecting data which arrived by way of the bottom. For this purpose, the depth of the isothermal layer, the decrease of the propagation-loss anomaly with range, the constancy of the field with depth, the magnitude of the propagation loss, and the acoustic frequency were all considered. On Cruise TWELVE pulses were used with the result that it was fairly easy to distinguish energy coming via the bottom. Propagation conditions were generally good during this cruise, however, and because only those signals which were less than 40 db below the direct signal could be detected, data were limited to a few stations.

All the AMOS data were assembled into median values, and the bottom loss was plotted against the bottom grazing angle in 5-degree intervals and out to 55 degrees as shown in Fig. 1. The geomet-

rical path was used together with the temperature-dependent absorption coefficients presented in Study A in reducing the propagation-loss values to "bottom loss."

In order to carry the bottom-reflection analysis down in frequency, underwater siren runs from
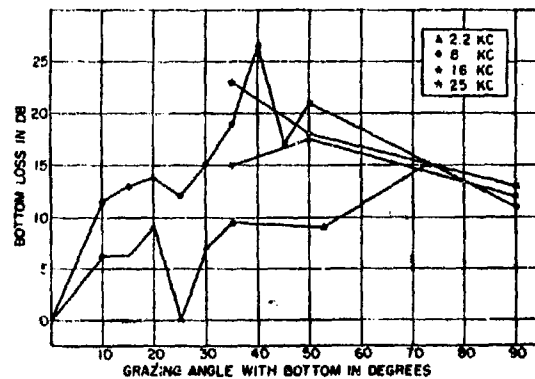
Fig. 1 - Bottom-Loss Data from AMOS Cruises NINE, ELEVEN, and TWELVE

AMOS Cruises ELEVEN and TWELVE were used. Data were considered in frequency bands centered about 1 kc, 2 kc, and 8 kc. Here again judgment had to be exercised in distinguishing bottom reflections, since the source emitted continuously. Bottom-reflection data, obtained by the Naval Electronics Laboratory during 1950 and 1951, were also available for discrete source runs at 500 cps and 1000 cps.[1] The medians for the siren and NEL runs are shown in Fig. 2. The number of runs going into these medians are as follows:

---

[1] These runs are described by T. P. Condron and R. W. Schillereff in "Long Range Sound Transmission with a Shallow Towed Source at 500- and 1000-cps Frequency," NEL Report 323, 16 October 1952 (UNCLASSIFIED).

33
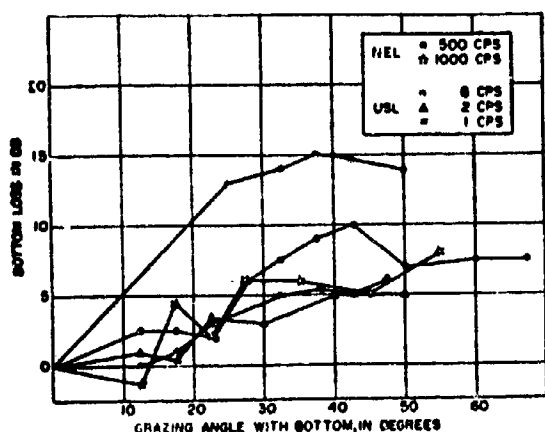
Fig. 2 - Bottom-Loss Data from NEL Discrete Source and USL Siren

Fig. 3 - Bottom-Loss Data from WHOI Bomb Drops

a. AMOS Underwater Siren--5 runs at 1 kc, 4 runs at 2 kc, 3 runs at 8 kc.

b. NEL Discrete Source--4 runs at 1 kc and 6 runs at 500 cps.

Finally, bottom-reflection data[2] obtained by the Woods Hole Oceanographic Institution at frequencies below 1 kc through bomb drops were derived for multiple-hop levels for energy lying between the limiting ray and the critical angle. In working out the data, all possible differences in level were used from the WHOI plots of level versus R/N, where R is the range and N is the order of reflection. Values of N from 1 to 9 were used. The median values of the resulting data are plotted in Fig. 3.

These three sets of data were studied for frequency dependence by plotting median bottom-reflection loss against frequency for the overlapping grazing angle intervals, 10° to 30°, 20° to 40°, and 30° to 50°. The results are shown in Figs. 4A, 4B, and 4C. In drawing smooth curves through the points, the AMOS data were given the greatest weight whenever a question arose. The source of the data is indicated by a letter W for WHOI, N for NEL, S for Siren (AMOS), and A for AMOS.

Plots of bottom loss versus grazing angle then were made, starting at 125 cps and progressing in octave steps. These are presented in Fig. 5. A

plot was also made at 25 kc for convenience. The points at 90° (vertical incidence) were obtained from a previous analysis[3] of the AMOS vertical reverberation and bottom-reflection experiments. The pulse-length dependence shown in the study indicates a tendency toward a leveling off at lower bottom-loss values with greater pulse lengths. The pulse data of AMOS Cruise TWELVE also shows a tendency toward lower levels for shorter pulses (i.e., 1/2 sec as compared with 1 sec).

Probable errors of the points about the curves in Figs. 4A, 4B, and 4C were computed and combined with the probable errors of the plots in Figs. 1, 2, and 3 in order to obtain the over-all probable-error curve versus frequency shown in Fig. 6. Finally, a plot of transmission loss versus horizontal range is presented in Fig. 7 for an average water depth of 2000 fathoms and average water temperature of 38° F. for the four frequencies indicated.

THEORETICAL COMPUTATIONS

Theoretical computations on the basis of two simple models were made in order to observe some dependencies of reflection coefficient on bottom property and bottom structure. In one case consider plane acoustic waves in one infinite, homo-

[2] See C. B. Officer and J. B. Hersey, "Sound Transmission from Deep to Shallow Water," WHOI Ref. 53-32, August 1953 (CONFIDENTIAL).

[3] See D. L. Cole, J. F. Kelly, and A. W. Dantuono, "Vertical Reverberation and Bottom Strength Measurements - Event SIX - Project AMOS," USL Technical Memorandum No. 1110-014-53, 15 May 1953 (CONFIDENTIAL).

34
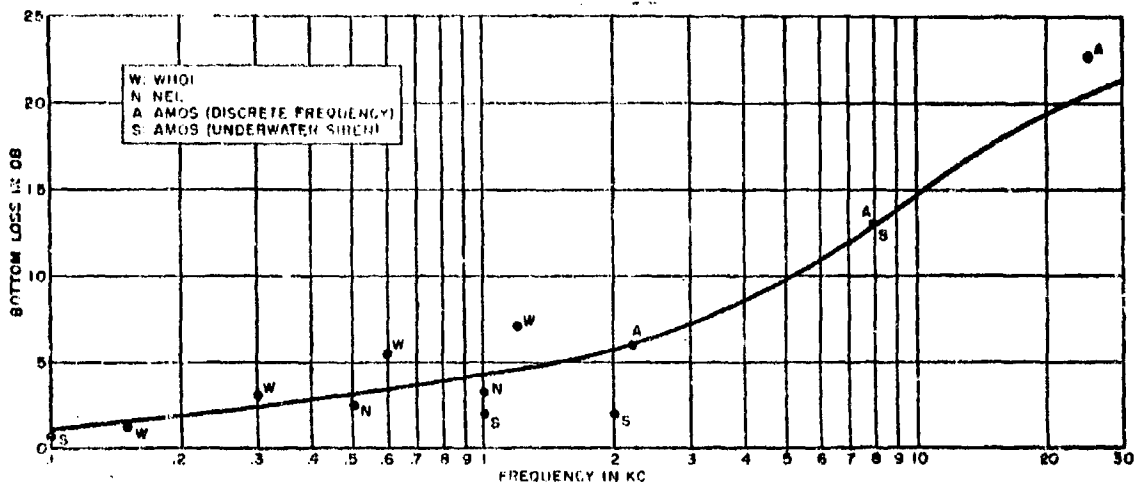
Fig. 4A - $10° \leq \theta_B \leq 30°$
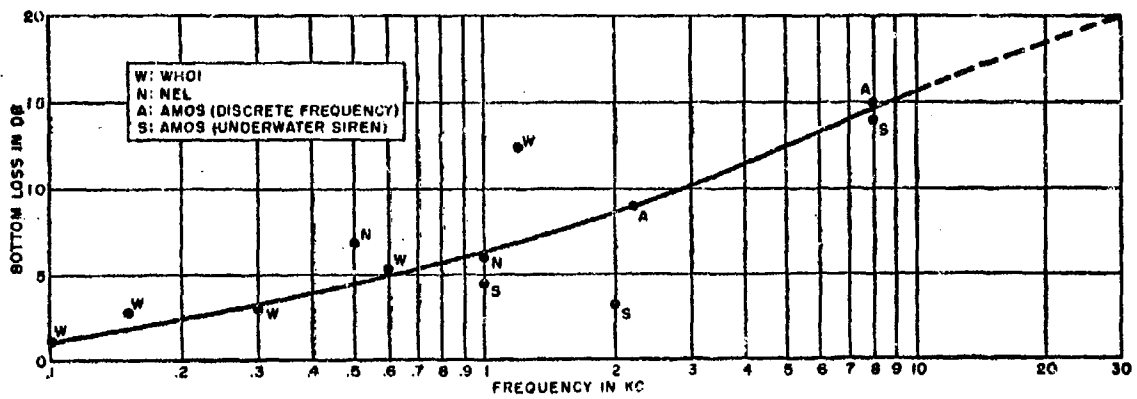
Fig. 4B - $20° \leq \theta_B \leq 40°$
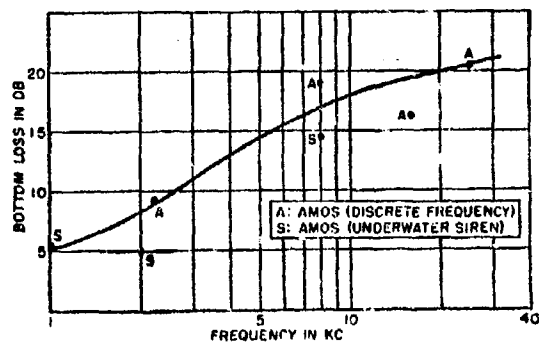
Fig. 4C - $30° \leq \theta_B \leq 50°$

Fig. 4 - Bottom Loss vs. Frequency
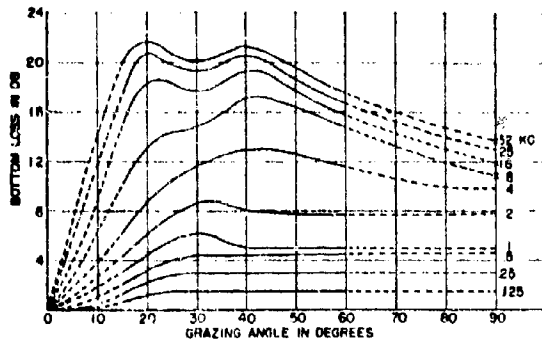
Fig. 5 - Bottom Loss vs. Grazing Angle

Fig. 8 - Rayleigh Theoretical Bottom Loss
vs. Grazing Angle (ρ, c constant)
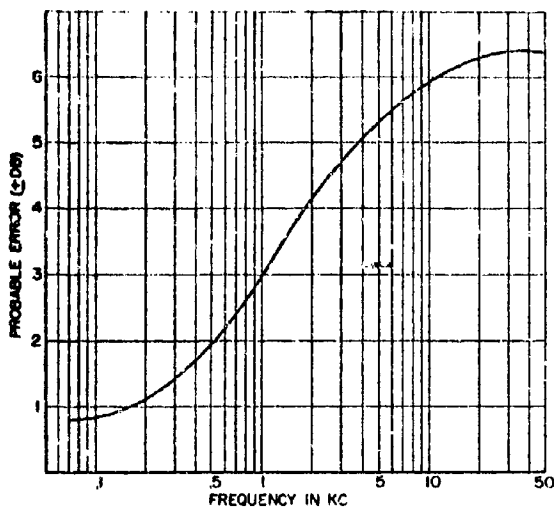
Fig. 6 - Probable Error in Bottom Loss vs. Frequency
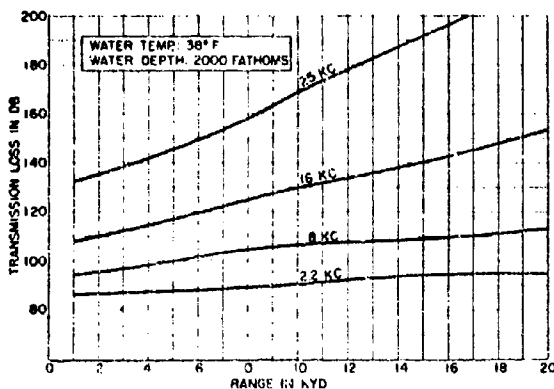
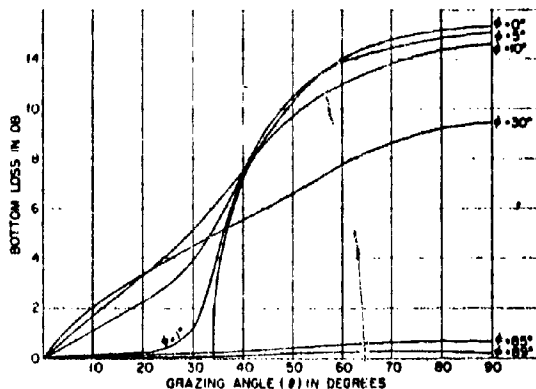Fig. 7 - Transmission Loss vs. Range for
Bottom-Reflected Transmission

geneous, fluid medium (sea water) impinging on the surface of separation for a second infinite, homogeneous, fluid medium (the bottom). In the second case consider that the bottom is composed of an absorbing fluid overlying a hard, perfectly reflecting surface.

In the first case the Rayleigh formula for the energy reflection coefficient is:

$$R_E = \left| \frac{\zeta \sin \theta_g - \sqrt{1 - \cos^2\theta_g (c_2/c_1)^2}}{\zeta \sin \theta_g + \sqrt{1 - \cos^2\theta_g (c_2/c_1)^2}} \right|^2 , \qquad (1)$$

where

$\theta_g \equiv$ grazing angle with bottom and

$\zeta = \rho_2 c_2 / \rho_1 c_1$.

Here, c_2 is complex and c_1 is the speed of sound in sea water; then

$$c_2 = |c_2| (\cos \phi - i \sin \phi) = |c_2| e^{-i\phi} .$$

In Fig. 8, the reflection coefficient is plotted against the grazing angle for a number of phase angles, ϕ, for the sound speed in the bottom. For the purposes of calculation, typical density ratios of $\rho_2/\rho_1 = 1.3$ and for $|\zeta| = 1.555$ were used. The main features of these curves are that (1) when the phase angle ϕ is close to zero, there is a critical angle of about $34°$ for which there is total reflection for all grazing angles up to this value; (2) for grazing angles of $5°$ and $10°$ the reflection coefficient decreases continuously in the "region of

36
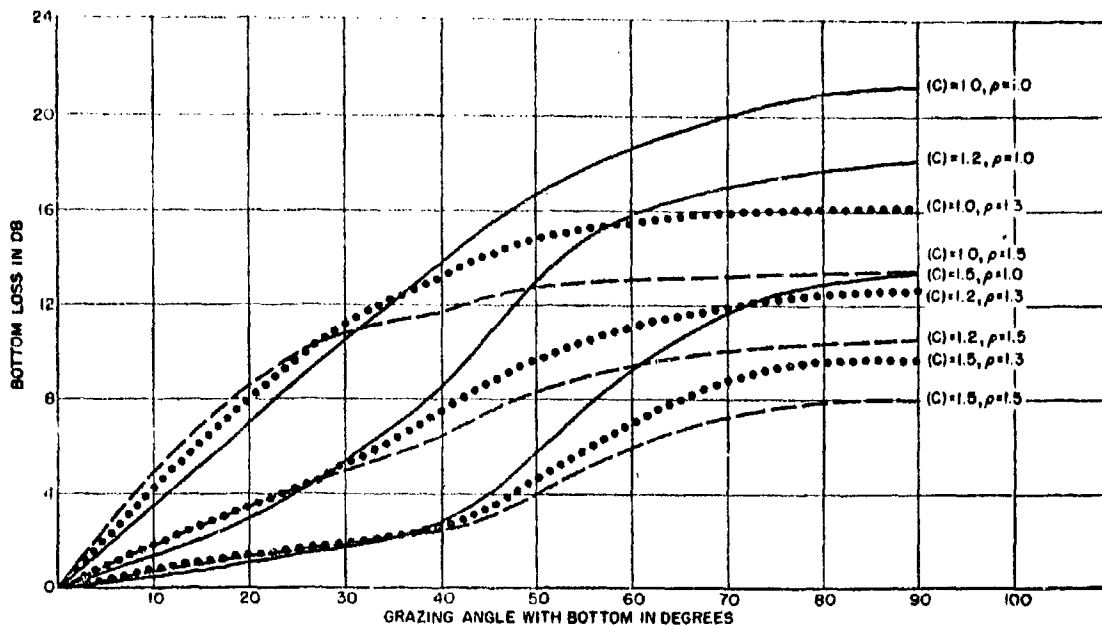
Fig. 9 - Rayleigh Theoretical Bottom Loss vs. Grazing Angle (Phase Angle constant)

total reflection," *i.e.*, there is no region of total reflection; and (3) as the phase angle increases from 30° to 90° the reflection coefficient improves steadily and the grazing angle dependence for each phase angle is continuous.

In Fig. 9, the phase angle is kept fixed at $10°$, and the variation of reflection coefficient with sound speed ratio is computed for different density ratios. It may be seen that the better matched the two media are, the poorer is the reflection coefficient. The purpose of computing these curves is to find the actual magnitudes involved. It may be seen that the previous model does not show the main features of the observed reflection coefficient data except at very low frequencies.

At the higher frequencies, there is an increase in reflection coefficient at greater grazing angles that needs explaining. The shape of the reflection coefficient curves at higher frequencies may be accounted for in various ways. For example, it may arise from a predominant specular reflection at small grazing angles and a predominant scattering effect at high grazing angles. Another possibility is that in the deep ocean a sound absorbing sediment layer overlies a harder, perfectly reflecting sediment which will accentuate the behavior above a certain frequency. There is some reason to believe that this last model has some physical justification from studies of deep sea sediments.[4]

If a plane wave is incident on a bottom composed of a sound absorbing layer of thickness, D, overlying a hard, infinite medium, then it can be shown that the amplitude reflection coefficient is given by:

$$R_A =$$

$$\frac{\zeta \sin \theta_1 + (\sqrt{1 - (c_2/c_1)^2 \cos^2 \theta_1})\, i \tan (\omega D \sin \theta_2/c_2)}{\zeta \sin \theta_1 - (\sqrt{1 - (c_2/c_1)^2 \cos^2 \theta_1})\, i \tan (\omega D \sin \theta_2/c_2)} \quad (2)$$

where

$$\sin \theta_2 = \sqrt{1 - (c_2/c_1)^2 \cos^2 \theta_1}.$$

[4] See Table 121, p. 1039, of *The Oceans* by H. U. Sverdrup, M. W. Johnson, and R. H. Fleming, Prentice-Hall, Inc., 1942.

37
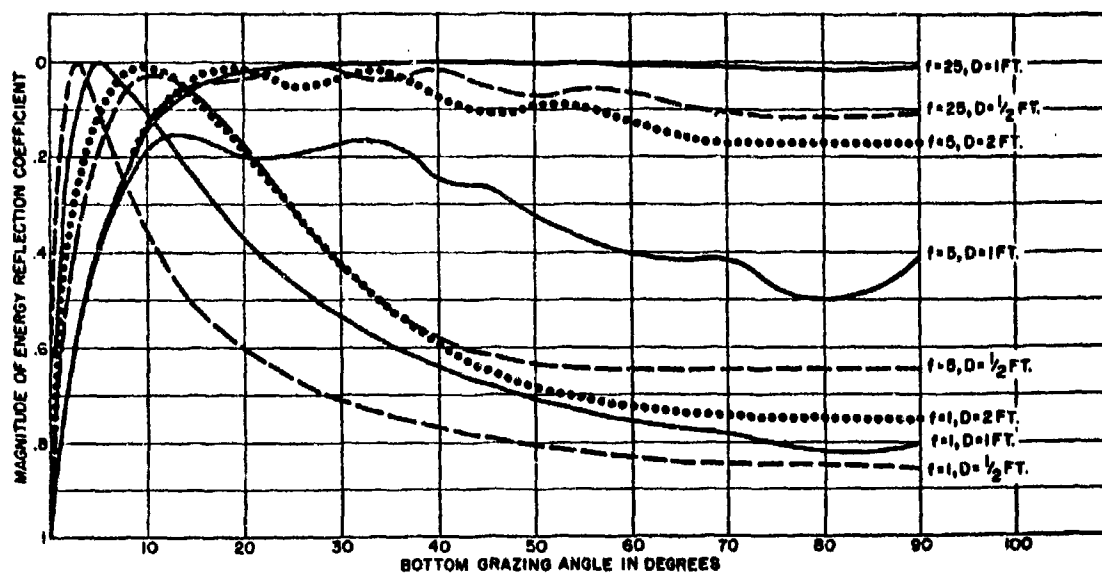
Fig. 10 - Magnitude of Energy Reflection Coefficient vs. Bottom Grazing Angle

38
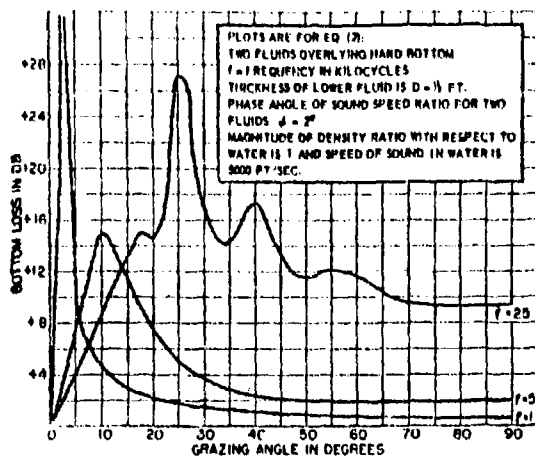
Fig. 11A - Second Fluid Thickness = ½ foot
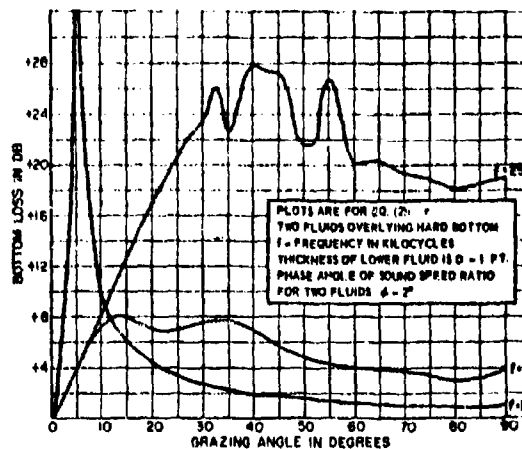
Fig. 11B - Second Fluid Thickness = 1 foot
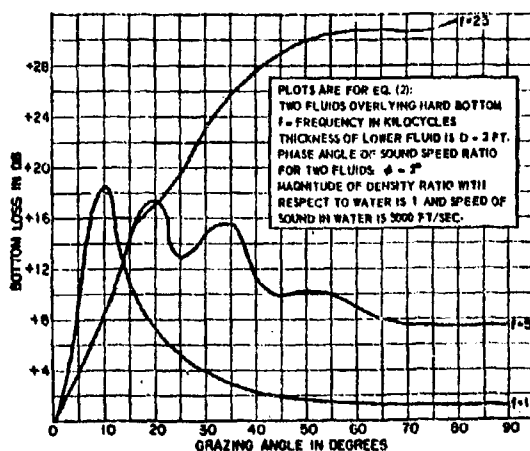
Fig. 11C - Second Fluid Thickness = 2 feet

Fig. 11 - Computed Bottom Loss vs. Bottom Grazing Angle

For the purposes of computation,

$$\phi = 2°,$$

$$C_1 = 5000 \text{ ft/sec},$$

$$C_2 = C_1 - iC_1 = \sqrt{C_1^2 + C_1^2}\, e^{-i\phi}, \text{ and}$$

$$|C_2| = C_1/\cos \phi.$$

In Fig. 10, the square of the absolute value of the reflection coefficient is plotted against grazing angle for various products of f and D. These are replotted in Figs. 11A, 11B, and 11C in terms of reflection loss in db. It may be seen that the shape of the curves and order of magnitude of reflection loss at the higher frequencies are suggestive of the average measured behavior. At the lower frequencies the simple, two-fluid model computations in Fig. 8 look like the measured curves in Fig. 5. The computations are merely meant to be suggestive of possibilities rather than to be applicable to the data.

39

Studies E Through G (pp. 40/64)
Are Classified Information and Are Omitted
from this Unclassified Edition of USL
Report No. 255 (CONFIDENTIAL).

40-64

STUDY H

THE USE OF RAY METHODS AND FIRST-ORDER DIFFRACTION CORRECTIONS[1]

by

H. W. Marsh, Jr.

INTRODUCTION

In many wave problems, ray methods are convenient and accurate. Exact in the limit of high frequency, and employing simple formulas, these methods lose utility at low frequencies or because of inadequate numerical schemes for interpreting them. We shall give correction terms which permit an extension of ray methods to lower frequencies (and at the same time provide an estimation of the validity of the high-frequency limit), and also set forth some useful formulas and numerical schemes for ray tracing and the quantitative evaluation of refraction (spreading) and interference.[2]

FORMULATION OF
THE RAY AND WAVE THEORIES

Throughout we consider an inhomogeneous medium in which the phase velocity varies in one direction only. With respect to a given Cartesian frame, let c_o be the phase velocity at the origin and c that at other points. Take c to be independent of x, y so that $c = c(z)$. Define the index of refraction to be

$$n = c/c_o. \qquad (1)$$

For waves of angular frequency ω, the wave number at the origin is k_o ($= \omega/c_o$), and the wave number at any point is

$$k = \omega/c = k_o/n. \qquad (2)$$

We shall characterize a field point P by its Cartesian coordinate (x, y, z), or its cylindrical coordinates (r, δ, z), or its polar coordinates (R, δ, β). Our interest will be devoted to cases of symmetry about the z axis. In such cases, the wave potential (of simply harmonic waves) can be expressed[3] in terms of cylindrical waves:

$$\phi = k_o \int_0^\infty F(ru)e^{-ik_o[ur - V(u, z)]} \, du$$

$$= k_o \int_0^\infty F(ru)e^{-i\psi} \, du. \qquad (3)$$

From the ray point of view, energy travels through the medium along paths described by the equation

$$dr/dz = n \cos \theta_o / \sqrt{1 - n^2 \cos^2 \theta_o}. \qquad (4)$$

Here θ_o is the inclination of the ray at the origin. Then, if θ is the inclination at any point on this ray, Snell's law is

$$\cos \theta = n \cos \theta_o. \qquad (5)$$

Combining Equations (4) and (5), we may write

$$r = \int_0^z \cot \theta \, d\zeta, \qquad (6)$$

The travel time along this ray is

$$t = \int_0^z (\quad \sin \theta) \, d\zeta, \qquad (7)$$

which may also be written

[3] $F(ru)$ is related to the zeroth order Bessel function by $F(ru) = J_o(ru)e^{ik_o ur}$ while $e^{ik_o V}$ is a one-dimensional wave function, satisfying
$$[(d^2/dz^2) + k^2 - k_o^2 u^2]e^{ik_o V} = 0.$$

$$c_o t = r \cos \theta_o + \int_0^z (\sin \theta / n) \, d\zeta. \qquad (8)$$

We may interpret the progressive divergence of a ray bundle as a corresponding spreading of wave energy. Thus, for a simple source behaving like $e^{-ik_o R}/R$ near the origin, we have from this point of view

$$I^{-1} = -(m \tan \theta) \, dr/d\theta_o \qquad (9)$$

as the ratio of wave intensity at unit distance from the origin to the intensity at other points on the ray.

ASYMPTOTIC DEVELOPMENT
OF THE WAVE FIELD

Equation (9) will break down when I^{-1}/r^2 is small. In order to investigate this situation, we may appeal to an asymptotic development of Equation (3). It is assumed that $F(ru)$ is but slowly varying. Considering an extension of the method of stationary phase, write

$$\psi(u) = k_o[ur - \nu(u, z)]$$

$$= \psi_o + (u - u_o) \, \psi_o' + (u - u_o)^2 \, \psi_o''/2$$

$$+ (u - u_o)^3 \, \psi_o'''/6 + \cdots \qquad (10)$$

as the Taylor series for $\psi(u)$ about the point u_o. Then

$$\psi_o = k_o u_o r - k_o \nu_o,$$

$$\psi_o' = k_o r - k_o \nu_o',$$

$$\psi_o'' = -k_o \nu_o'',$$

$$\psi_o''' = -k_o \nu_o'''. \qquad (11)$$

The stationary point u_o is the solution of the equation $\psi_o' = 0$. Therefore,

$$r = \nu_o'. \qquad (12)$$

Equation (12) is simply the equation of that ray for which $u = \cos \theta_o$. Now in Equations (11), r and z are fixed. If we write r' for $dr/d \cos \theta_o$, where r satisfies (12) and z is held constant, we then have

$$\psi_o = \omega t,$$

$$\psi_o' = 0,$$

$$\psi_o'' = -kr',$$

$$\psi_o''' = -kr''. \qquad (13)$$

Here ψ_o/ω turns out to be the travel time along the ray in question, and the "ray intensity," Eq. (9), is simply related to the rate of change of this time.

According to the method of stationary phase, we can now write

$$\phi \sim k_o e^{-i\omega t} \, F(r \cos \theta_o)$$

$$\times \int e^{i(k_o/2) [u^2 r' + (u^3/3) r'']} du. \qquad (14)$$

The path of integration in Eq. (14) is to pass through the point $u = 0$ and is to terminate at infinity in such a manner that the integral converges absolutely for general values of $k_o r'$ and $k_o r''$. We shall presume that both these quantities have a small non-negative argument, with results for other values following by analytic continuations.

An appropriate path of integration is Γ, as illustrated in Fig. 1.
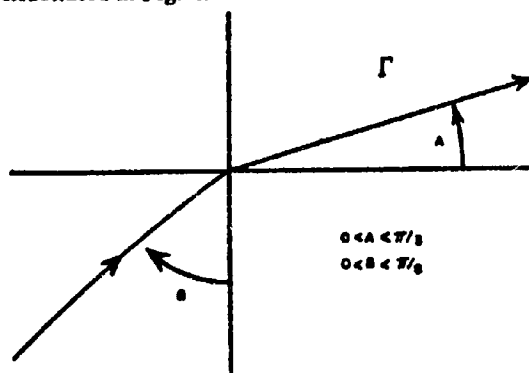
Fig. 1 - Path of Integration, Γ

66

By a linear transformation of the variable of integration u, and an appeal to Cauchy's theorem, we get

$$\phi \sim (2/k_o r')^{1/3} k_o P(r \cos \theta_o)$$

$$\times e^{-i(\omega t + \pi/6 - k_o r'^3/3r''^2)}$$

$$\times \int_{\Gamma'} e^{uv + v^3/3} dv, \tag{15}$$

where

$$w = \mathcal{Z}^{2/3} e^{-2\pi i/3} (k_o r')^2/(k_o r'')^{4/3}. \tag{16}$$

and Γ' is as indicated in Fig. 2. The contour in Fig. 3 is equivalent to the contour in Fig. 2. By considering the contour in Fig. 3 and referring to the appropriate tables,[4] it is found that
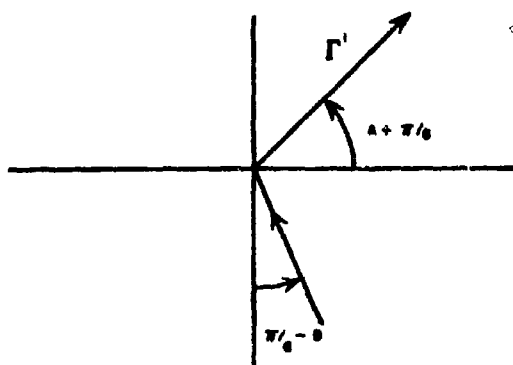
Fig. 2 - Transformed Path of Integration, Γ'
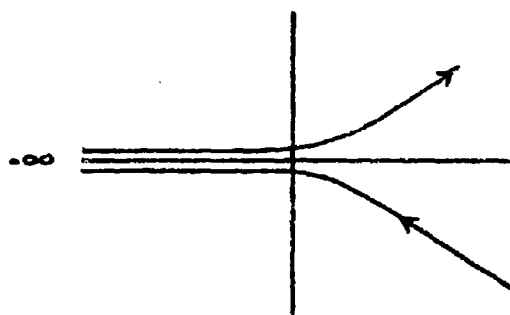
Fig. 3 - Equivalent Contour for Path of Integration, Γ'

---

[4] Tables of the Modified Hankel Functions of Order One-Third, Computation Laboratory, Harvard University.

$$\phi \sim (2/k_o r'')^{1/3} k_o P(r \cos \theta_o)$$

$$\times e^{-i(\omega t + \pi/6 - k_o r'^3/3r''^2)}$$

$$\times (\pi/12^{1/6}) \, h_2 \{(k_o/2)^{2/3} r'^2/r''^{4/3}\}. \tag{17}$$

For large k_o, this is asymptotically

$$\phi \sim [k_o^{1/2}/(r')^{1/2}] P(r \cos \theta_o) (2\pi i)^{1/2} e^{-i\omega t}, \tag{18}$$

which is equivalent to Eq. (9), i.e., in the optical limit ($k_o \to \infty$). This method of stationary phase reduces to the geometrical, or ray, approximation. Let ϕ_o denote this limiting form of ϕ. Then we may write in general

$$\phi = \phi_o \frac{e^{i(k_o r'^3/3r''^2 - 5\pi/12)} \pi^{1/2} (k_o r')^{1/2}}{2^{1/2} 3^{1/6} (k_o r'')^{1/3}}$$

$$\times h_2 \{(k_o/2)^{2/3} r'^2/r''^{4/3}\}, \tag{19}$$

or writing

$$a = k_o r'^3/2r''^2, \tag{20}$$

and

$$\phi = \phi_o J(a), \tag{21}$$

we have

$$J(a) = e^{i(2a/3 - 5\pi/12)/2^{1/3} 3^{1/6}}$$

$$\times \pi^{1/2} a^{1/6} h_2 \{a^{2/3}\}. \tag{22}$$

For $a \to \infty$, implying high frequencies, $J(a) \to 1$. Conversely, for $a \to 0$, implying low frequencies, or near caustic lines,

$$J(a) \to 2\pi^{1/2} e^{\pi i/12} a^{1/6}/3^{2/3} \Gamma(2/3), \tag{23}$$

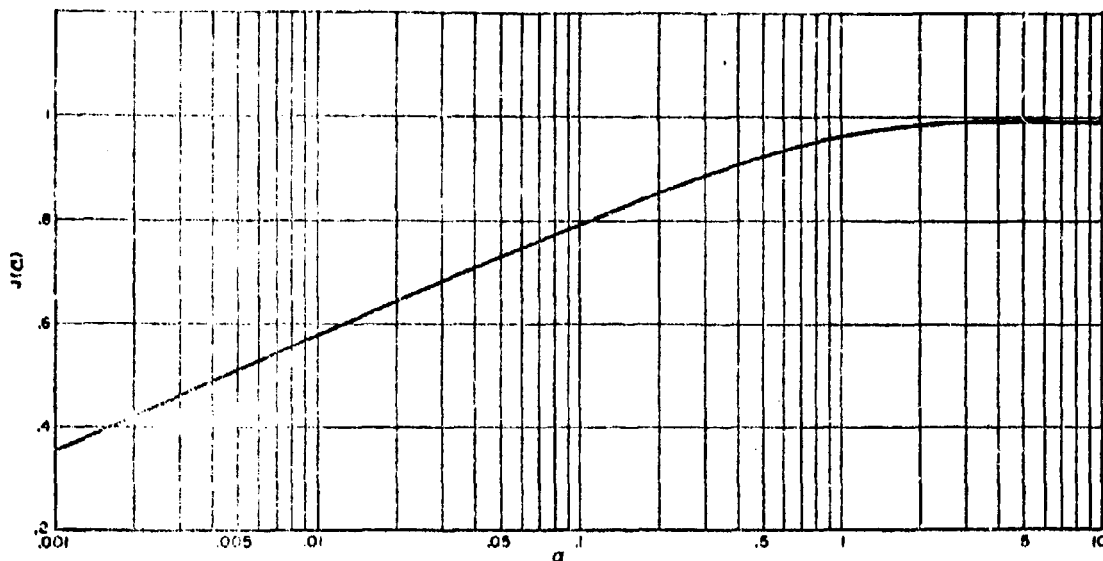and taking into account Eq. (9), ϕ in this limit is

Fig. 4 - First-Order Diffraction Correction

$\phi = 2^{4/6} \, \pi^{1/2} \, e^{\pi i/12}/3^{2/3} \, \Gamma(2/3)$

$\times [k_0^{1/6}/(r'')^{1/3}](\sin \theta_0/m \tan \theta)^{1/2} .$ (24)

A graph of $J(a)$ is given in Fig. 4. It is to be noted that J is indifferent to the sign of r'' and that the conjugate value of J is to be employed when r' is negative.

A SIMPLE METHOD
OF PREDICTING INTERFERENCE

The exact travel time along a single ray is seldom important. On the other hand, the difference of travel times along intersecting, and hence interfering, rays is often of interest. A significant feature of this interference is its change with distance. For example, the spacing between interference nulls is a most enlightening feature of the pattern.

Referring to Eq. (8), we have for constant z,

$dt/dr = (dt/d \cos \theta_0) \, a \cos \theta_0/dr$

$= 1/c_0 \, [(dr/d \cos \theta_0) \cos \theta_0 + r$

$+ \int_n^r u \cos \theta \, (d\theta/d \cos \theta_0) \, dz]$

$\times d \cos \theta_0/dr$

$= \cos \theta_0/c_0 ,$ (25)

where we have also used Eqs. (5) and (6). We then have

$d^2t/dr^2 = - (\sin \theta_0/c_0) \, d\theta_0/dr$

$= m \sin \theta_0 \tan \theta l/c_0 .$ (26)

Now, except near focusing regions, $l \sim r^{-2}$, so that d^2l/dr^2 will normally be negligibly small. Thus, if Δt is the difference of travel times between rays with source inclinations θ_0, θ_0', the change in Δt over a change Δr in distance will be nearly

$(\Delta r/c_0)[\cos \theta_0 - \cos \theta_0'] .$ (27)

68

Therefore, the spacing between points of similar interference characteristics is nearly

$$(2\pi c_o)/\omega \left[\cos\theta_o - \cos\theta_o'\right]. \qquad (28)$$

This approximation is valid when $t \sim r^2$ and when $r \gg \Delta r$. Its great utility comes from the fact that only the ray inclinations at the source need be known.

In cases where θ_o and θ_o' are nearly the same, Δt itself can be found simply. Consider the situa-
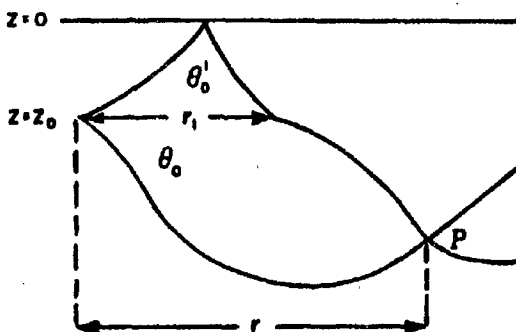

Fig. 5 - Two Ray Paths for Computation of Travel-Time Difference

tion illustrated in Fig. 5. The travel time difference, using Eq. (8), is

$$\Delta t = r_1 \cos\theta_o'/c_o + (2/c_o)\int_0^{z_o}(\sin\theta'/n)\,d\zeta$$

$$+ (1/c_o)\int_{z_o}^{z}(\sin\theta'/n)\,d\zeta$$

$$- (1/c_o)\int_{z_o}^{z}(\sin\theta/n)\,d\zeta + (r - r_1)\cos\theta_o'/c_o$$

$$- r\cos\theta_o/c_o. \qquad (29)$$

The first two terms represent the travel time t_1 of the primed ray in the medium above the source. The remainder of Δt is the difference in time for two rays of inclination θ_o, θ_o' traversing the same medium, to distances r and $r - r_1$, respectively. This remainder is nearly

$$(dt/d\theta_o)(\theta_o - \theta_o'),$$

and the angular difference $\theta_o - \theta_o'$ is nearly

$$(d\theta_o/dr)\,r_1.$$

Hence,

$$\Delta t \sim t_1 + (r_1/c_o)\,dt/dr = t_1 + r_1\cos\theta_o/c_o. \qquad (30)$$

Equation (30) is useful when $\theta_o - \theta_o'$ is small. When this is true, r_1 can be computed using θ_o in lieu of θ_o', so that the actual angle θ_o' need never enter into the calculation. If greater accuracy is required, Eq. (30) can easily be extended to higher-order terms, which will involve, for example, the ray intensity and its rates of change. Therefore, the tracing of the basic ray, together with its first and second space or angular derivatives, will usually yield complete practical information on refraction (spreading), diffraction, and interference.

STRATIFIED MEDIA—SPECIAL CASES

In creating a problem involving an arbitrary index of refraction, it is usual to divide the medium up into strata, in each of which n varies in a simple manner. Ray tracing then consists of applying formulas to get the increments of distance, travel time, and intensity in each stratum, and proper combination of these to yield the properties of the entire ray. Thus, let z_i be the thickness of the ith stratum, r_i and t_i, the increments of distance and travel time in the stratum, and θ_i the angle at which the ray enters. Then

$$r = \Sigma r_i,$$

$$t = \Sigma t_i,$$

$$t^{-1} = -(r\sin\theta/\cos\theta_o)\Sigma(dr_i/d\theta_o).$$

Table 1 below gives formulas which apply to several forms of variation of n. In the table, c_i is the velocity at the point of entry of the ray, and n_i is c/c_i.

69

Table 1

FORMULAS APPLICABLE TO VARIOUS RAY SHAPES

n	r_i	t_i	Geometrical Form of Ray
$1 + gz$	$x_i \cot[(\theta_o + \theta_i)/2]$	$(1/c_i g_i)[\sinh^{-1}\tan\theta_i - \sinh^{-1}\tan\theta_o]$	Circle
$1/\sqrt{1-(g/2)z}$	$4/g_i n_i \sin(\theta_i - \theta_o)$	$(1/c_i)[r_i \cos\theta_i - 4\sin^3\theta_o/3g_i n_i + 4\sin^3\theta_i/3g_i]$	Parabola
$1/\sqrt{1 - g^2 z^2}$	$(\cos\theta_i/g_i)\sin^{-1}(g_i x_i/\sin\theta_i)$	$(r_i/2c_i\cos\theta_i)[1 + \cos^2\theta_i] + x_i \sin\theta_i/2c_i n_i$	Sine Curve

TABLES FOR RAY DIAGRAMS

A set of tables, which are useful in tracing rays through stratified media, in which the separate strata have constant velocity gradients, has been prepared on IBM equipment. These tables provide travel time, distance, and intensity increments. Entry into the tables is accomplished through the angle θ_o of entry of the ray and the index of refraction n. Divided differences are provided. Linear interpolation, using these differences, will give sufficient accuracy for most purposes. The tables cover the ranges for θ_o in degrees.

$$\theta_o = \begin{Bmatrix} 1[0.1] 2 \\ 2[0.2] 5 \\ 5[0.5] 10 \end{Bmatrix} \times 10^m, \quad m = -1, 0, 1$$

$n = 1.00002 [0.00002] 1.002$
$\quad 1.002 [0.002] 1.01$
$\quad 1.01 [0.01] 1.1$

to give the following tabulated quantities:

θ_1 : $\cos\theta_1 = n\cos\theta_o$

ρ : $\cot[(\theta_o + \theta_1)/2]$

τ : $(\sinh^{-1}\tan\theta_o - \sinh^{-1}\tan\theta_1)/(n - 1)$

δ : $\rho/\sin\theta_o \sin\theta_1$.

Using these, and the notation of the preceding section, we have

$r = \Sigma \rho_i x_i$,

$t = (1/c_o) \Sigma \tau_i x_i$,

$I^{-1} = (\sin\theta \cdot \sin\theta_o r/\cos^2\theta_o) \Sigma x_i \delta_i$.

These tables are available at the Laboratory either in tabulated form or on IBM cards.

STUDY I

AMOS LOW-FREQUENCY DATA-ANALYSIS METHODS[1]

by

T. P. Condron and J. F. Kelly

AMOS LOW-FREQUENCY
DATA-ANALYSIS METHODS

INTRODUCTION

One of the objectives of the AMOS low-frequency acoustic measurements is the determination of attenuation values in the frequency range from approximately 100 to 8000 cycles per second as a function of the mode of propagation. In pursuit of this objective, a total of 28 low-frequency acoustic stations were included during AMOS Cruises ELEVEN and TWELVE. The objectives of this report are to discuss a semiautomatic analysis system which was developed at the Underwater Sound Laboratory in order to process the data from these stations and to present sample plots which were made by the system and which point up one of the more important modes of propagation.

The data to be processed are in the form of broad-band dual-channel magnetic-tape recordings made at sea by the listening AMOS ship while the transmitting ship operated an underwater siren or Mk 4(v) hammerbox and opened range to 80 kiloyards. Each tape-recorder channel recorded the output of a hydrophone suspended at a depth of either 50 or 500 feet continually while the range was being opened.

METHOD OF ANALYSIS

A block diagram of the analysis system appears in Fig. 1. The purpose of the system is to resolve the broad-band signal into 10 narrow bands and to produce a plot of sound-pressure level as a function of the logarithm of the range for each band. In operation, the signal is fed from the magnetic tape to ten filters and then is averaged for three seconds in the rectifier averagers. The averaged output of each filter is then fed to one position of a Bell Telephone stepping switch, which is driven at such a rate that a given filter output is sampled once every 30 seconds. This is equivalent to a range increment of 150 to 250 yards, depending upon the speed of the transmitting ship. The signal for each filter is then fed to a Western Electric 4A Graphic Level Recorder, where a photoelectric reading head attached to the recorder shaft converts the voltages to a discrete number of pulses, which are fed to a binary counter and finally to an IBM Summary Punch. Thus, the averaged output of each filter is punched into an IBM card as the stepping switch rotates. After the cards are processed, they are fed to an X-Y Plotter, and the end result is a plot of sound-pressure level in decibels relative to one dyne per centimeter squared as a function of the logarithm of the range for each of the ten frequency bands. Most of the 28 stations taken to date have been processed by the system.
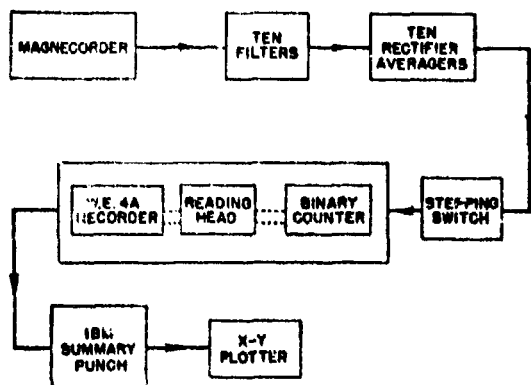
Fig. 1 - Block Diagram of Broad-Band Analysis System

RESULTS OF ANALYSIS

In order to indicate some of the general results of the analysis made to date, propagation curves for three stations made at fairly widely separated locations in the North Atlantic Ocean will be presented. The mode of propagation best emphasized by these curves is that responsible for the foci

which occur at 70-kiloyard intervals in the southern portions of the North Atlantic and Pacific Oceans and at shorter ranges at more northerly latitudes. The curves are presented primarily to show the variation of range to the focus with geographical location and the variation in signal increase at the focus with frequency.

In Fig. 2 are shown the sound-velocity—depth profile and a propagation plot for a station taken at 68° north latitude and 01° west longitude in August. Ray calculations indicate that rays having an inclination of less than 0.5° from a source at a depth of 50 feet would be retained in the shallow surface layer. Those having inclinations between 0.5° and 10° would be refracted down into the layer between the bottom of the SOFAR channel (dashed line) and the ocean bottom and would return to a hydrophone at a depth of 50 feet at ranges of between 45 and 53 kiloyards; the focus peak would occur at 46 kiloyards. Rays with inclinations greater than 10° would reflect from the ocean bottom and would be received at all ranges between the source and 45 kiloyards. The agreement between the predicted and observed focus range for the frequency band centered at 3600 cps is good.

Fig. 2A - Sound-Velocity—Depth Profile

SOURCE — SIREN   HYDROPHONE — 50 FT
FREQ — 3600 CPS   DEPTH
BAND- — 800 CPS   1 AUGUST 1952
WIDTH
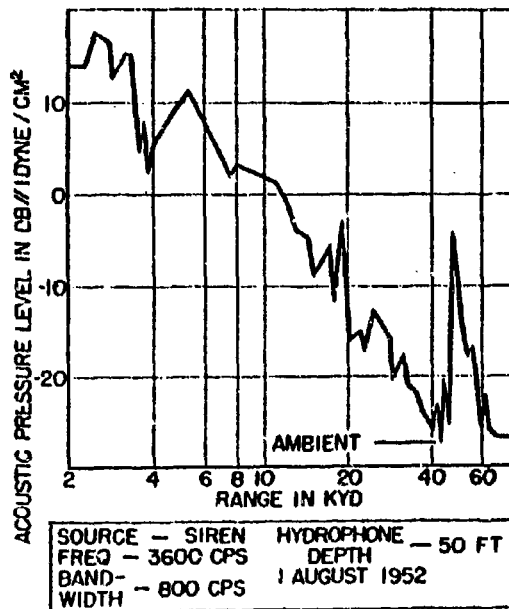
Fig. 2B - Propagation Curve

Fig. 2 - Data Obtained on Station 68° N, 01° W,
1 August 1952

SOUND VELOCITY IN FT/SEC

Fig. 3A - Sound-Velocity--Depth Profile

ACOUSTIC PRESSURE LEVEL IN DB//1DYNE/CM²

AMBIENT

RANGE IN KYD

SOURCE — SIREN	HYDROPHONE
FREQ. - 3600 CPS	DEPTH — 50 FT
BAND-WIDTH — 800 CPS	18 JULY 1952
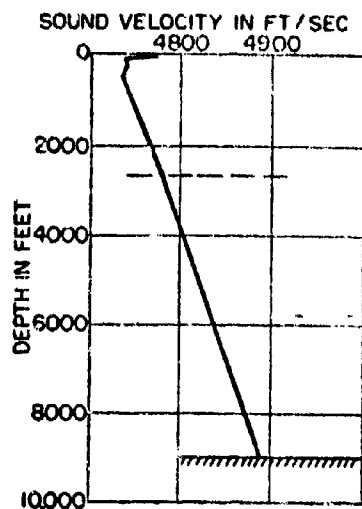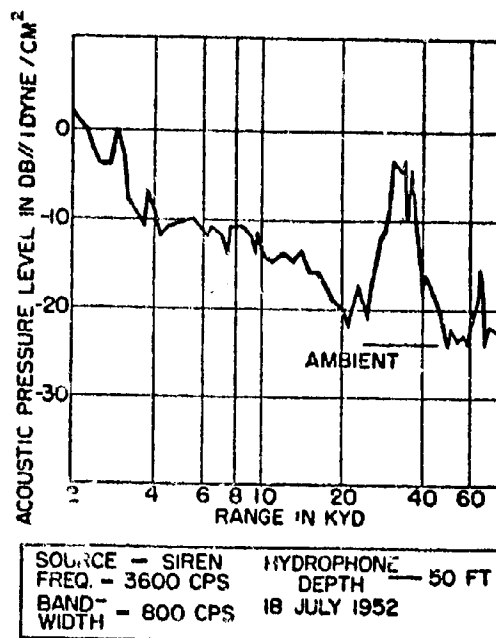
Fig. 3B - Propagation Curve

Fig. 3 - Data Obtained on Station 75° N, 01° E,
18 July 1952

SOUND VELOCITY IN FT/SEC
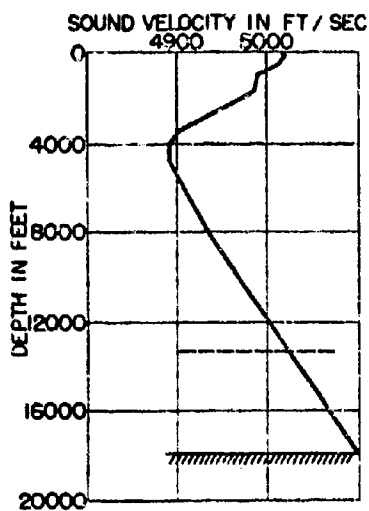
Fig. 4A - Sound-Velocity—Depth Profile
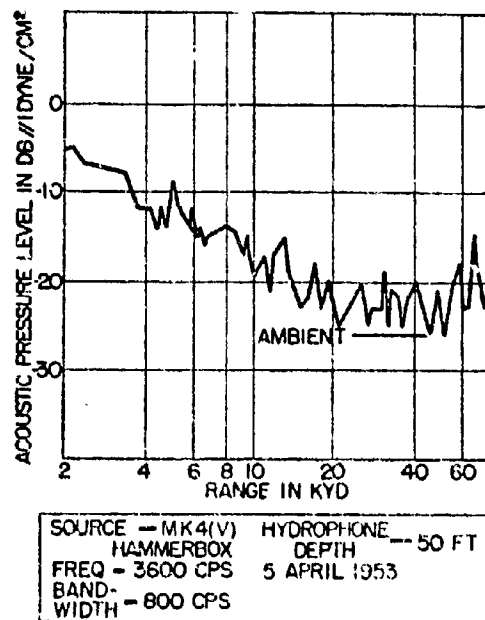
Fig. 4 - Data Obtained on Station 26° N, 70° W,
5 April 1953

ACOUSTIC PRESSURE LEVEL IN DB//1DYNE/CM²

AMBIENT

RANGE IN KYD

SOURCE — MK4(V) HAMMERBOX	HYDROPHONE DEPTH — 50 FT
FREQ - 3600 CPS	5 APRIL 1953
BAND-WIDTH - 800 CPS	

Fig. 4B - Propagation Curve

73

Data for Fig. 3 were obtained on a station located 7° north of the previous one, at 75° north latitude and 01° east longitude during July. Ray calculations for this situation indicate that rays having inclinations of 1.1° to 12.5° at the source depth would refract back to a depth of 50 feet at ranges of between 27 and 46 kiloyards, and the predicted focus peak would be at 29 kiloyards. Here again, there is good agreement between the predicted focus at 29 kiloyards and the observed peak, which begins at 31 kiloyards.

Figure 4 contains data taken on a station well south of the other two, at 26° north latitude and 70° west longitude during April. The Mk 4(v) hammerbox, which was used for this station, does not have so great an output as does the siren used on the previous two stations. In this instance, the predicted focus range is 70 kiloyards and the observed peak occurs at 69 kiloyards. Although this focus appears to be weaker than the other two, the total loss from 2 kiloyards to the focus is approximately 8 to 10 db less than in the previous two cases, and the apparent weakness is caused by a lower source output.

These three stations, for which focus peaks occurred at 48, 31, and 69 kiloyards, respectively, in the band from 3200 to 3800 cps, did not exhibit a marked focus at all frequencies. For purposes of comparison, the propagation plots presented in Figs. 2 through 4 are repeated in Figs. 5 through
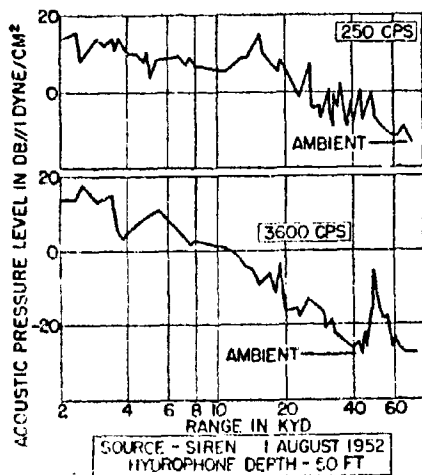
Fig. 5 - Comparison of Propagation Curves, 1 August 1952
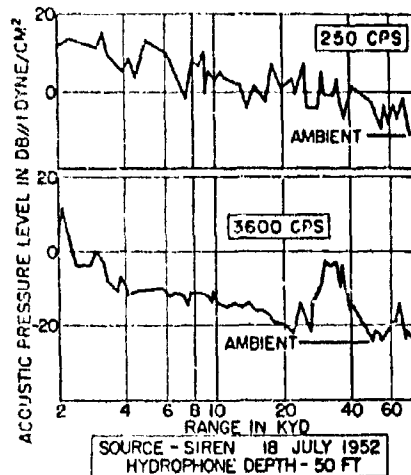
Fig. 6 - Comparison of Propagation Curves, 18 July 1952
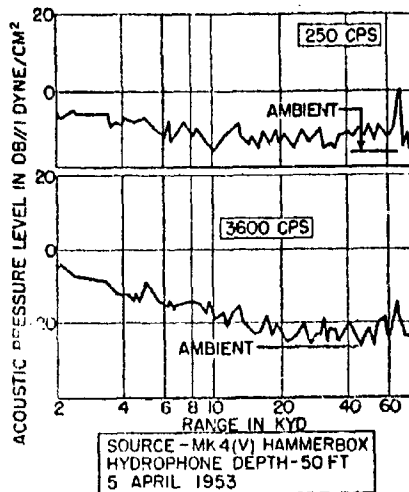
Fig. 7 - Comparison of Propagation Curves, 5 April 1953

7, accompanied by a plot for a 100-cps band centered at 250 cps.

Figure 5 represents the station where the focus was observed at 48 kiloyards. Although there is a rise in level of approximately 20 db for the band centered at 3600 cps, no marked level increase occurs at 250 cps. The same type of frequency behavior is observed for the second station, as is shown in Fig. 6. In Fig. 7, however, the rise at the focus is somewhat more pronounced at 250 cps than it is at 3600 cps.

74

CONCLUSIONS

No explanation for the dependence of focus intensity on frequency is offered at present, but it is interesting to note that the frequency band which best shows up a focus is not always the lowest one.[2] It is hoped that an analysis of explosive pulses used in conjunction with the siren and

Mk 4(v) hammerbox during these experiments will shed some light on this behavior.

The AMOS low-frequency program has reached a stage where a substantial number of experimental stations have been occupied, and the data from most of these stations have been processed. The propagation curves are now being interpreted in the light of environmental factors. However, in order to obtain the statistical averages which will be required for a practical application of the data, a much larger number of additional stations will be required.

---

[2] These conclusions were appropriate when the original study was prepared. An explanation of this phenomenon is presented in Study J.

STUDY J

COMPARISON OF COMPUTED AND MEASURED INTENSITIES
FOR PROJECT AMOS NOISEMAKER MEASUREMENTS[1]

by

T. P. Condron, D. L. Cole, and J. F. Kelly

Theoretical intensity-versus-range plots have been computed for one set of Project AMOS deep-water, low-frequency measurements. The sound field in the vicinity of caustics and the bottom-reflected field are included in the computations. These plots are compared with actual propagation runs for which a broad-band noisemaker covering the frequency range from 250 to 8000 cps was used. The observed intensities are in substantial agreement with theory.

During the propagation program which the Underwater Sound Laboratory has conducted for several years in connection with Project AMOS, a variety of acoustic measurements have been made. Of these measurements, the type to be discussed in this study will be those in which a listening ship lay to in deep water while a transmitting ship operated a noisemaker and opened range to approximately 80,000 yards.[2] The object of this discussion is to present the method being used to interpret the propagation loss observed for each of ten frequency bands in the light of oceanographic factors.[3]

In general, three major modes of propagation are responsible for the behavior of the observed signal versus range: (1) the direct sound field, which is always predominant at the short ranges; (2) the bottom-reflected field, which becomes predominant in the region beyond the direct field; and (3) the focused field, which is commonly observed at a range of about 60 kyd in the southern portions of the North Atlantic and Pacific Oceans and at shorter ranges in more northerly latitudes. For the direct and focused fields the major causes of signal reduction with range are spreading and absorption. For the bottom-reflected field, a boundary loss is introduced.

The first portion of this study will deal with the bottom-reflected field, and the final portion will be a discussion of the focused field. Since we are primarily interested in long-range propagation, it will suffice to state that the direct field terminates at a range of approximately 4 kyd for the station with which we are concerned. Measurements on this station were made by using an underwater siren in 1500-fathom water in the northern latitudes of the North Atlantic Ocean.

The expression for ratio of the intensity at one yard to that at any point in the medium (Eq. (9), Study H) may be written:

$$I^{-1} = (R \sin \theta / \cos \theta_0) \, dR/d\theta_0 \,, \tag{1}$$

where

θ_0 = the angle which the ray makes with the horizontal at the source,

θ = the angle which the ray makes with the horizontal at the receiver, and

R = the horizontal distance from the source to the receiver.

It is customary to break the velocity-depth curve into layers of constant gradient, and then

---

[1] This study was delivered as a paper at the Ninth Navy Symposium on Underwater Acoustics, at the Naval Research Laboratory in June 1954 and was subsequently published in the January 1955 issue of the *Journal of Underwater Acoustics.*

[2] This type of run is designated as a "station" and will be referred to as such throughout this study.

[3] The method which was used to resolve these noisemaker runs into plots of signal level versus range for ten frequency bands was discussed in "AMOS Low-Frequency Data Analysis Method," by Thomas P. Condron and John F. Kelly, a paper delivered at the Eighth Navy Symposium on Underwater Acoustics, at the Underwater Sound Laboratory, 19-20 November 1953. See also Study I of the present report.

$$R = \sum_{1}^{N} r_i$$

and

$$dR/d\theta_o = \sum_{1}^{N} dr_i/d\theta_o$$

for N layers. The formulas which were used for computing r_i and $dr_i/d\theta_o$ are as follows:

$$r_i = (c_o/g_i \cos \theta_o)(\sin \theta_i - \sin \theta_{i+1}) ; \qquad (2)$$

$$(dr_i/d\theta_o) = (c_o \sin \theta_o/g_i \cos^2 \theta_o)$$
$$\times (1/\sin \theta_i - 1/\sin \theta_{i+1}) . \qquad (3)$$

In the layer containing a vertex, the range from the depth where the ray enters the layer to the same depth on the other side of the vertex is

$$r_v = (2c_o/g_v \cos \theta_o) \sin \theta_v , \qquad (4)$$

and the derivative is

$$dr_v/d\theta_o = (2c_o/g_v \cos^2 \theta_o)(\sin \theta_o/\sin \theta_v) . \qquad (5)$$

In the above formulas g_i is the gradient in the ith layer, g_v is the gradient in the vertex layer, θ_v is the angle which the ray makes with the horizontal at the depth where it enters the vertex layer, and θ_i and θ_{i+1} are the angles made by the ray upon entering and leaving the ith layer.

Thus, at any point after the vertex:

$$dR/d\theta_o = (dr_v/d\theta_o)$$
$$+\left[\sum_{1}^{v-1}(dr_i/d\theta_o) - \sum_{v+1}^{N}(dr_i/d\theta_o)\right]. \qquad (6)$$

The $v-1$ and $v+1$ refer to the layers just before and after the vertex layer, respectively. When the sum of the terms inside the brackets of Eq. (6) becomes equal to $dr_v/d\theta_o$ in magnitude, then $dR/d\theta_o$ vanishes (since all the $dr_i/d\theta_o$ terms have the opposite sign from $dr_v/d\theta_o$) and a caustic is reached. However, a second derivative exists unless it is also a cusp, in which case the third derivative would be required.

The corrected intensity in the vicinity of a caustic is obtained by multiplying the ray inten-

sity by the square of a value obtained from Fig. 1. The value of the parameter is computed from the following relationship given in Eq. (20), Study H:
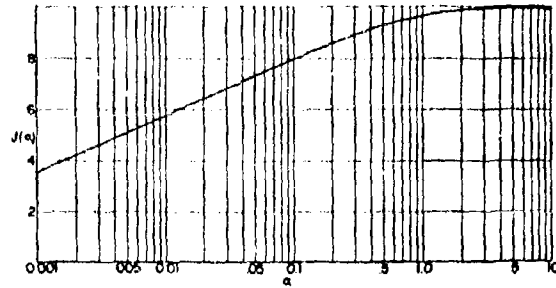
$$a = k_o (dR/dx)^3/2 (d^2R/dx^2)^2 , \qquad (7)$$

where x is $\cos \theta_o$ and k_o is the wave number at the source. $J(a)$ is given in Study H.

The derivatives appearing in Eq. (7) were computed layer by layer as follows:

$$dr_i/dx = -(c_o/g_i \cos^2 \theta_o)(1/\sin \theta_i - 1/\sin \theta_{i+1})$$
$$= -(1/\sin \theta_o)(dr_i/d\theta_o) .$$

$$dr_v/dx = -(2c_o/g_v \cos^2 \theta_o)(1/\sin \theta_v)$$
$$= -(1/\sin \theta_o)(dr_v/d\theta_o), \qquad (8)$$

$$d^2r_i/dx^2 = (c_o/g_i \cos^3 \theta_o)$$
$$\times [(1/\sin^3 \theta_i - 1/\sin^3 \theta_{i+1})$$
$$- (3/\sin \theta_i - 3/\sin \theta_{i+1})],$$

$$d^2r_v/dx^2 = (c_o/g_v \cos^3 \theta_o)$$
$$\times (1/\sin^3 \theta_v - 3/\sin \theta_v). \qquad (9)$$

For purposes of illustrating the method which was used to compute phase, two rays which reflect from the bottom will be considered with the source

78

$R_{\theta_{02}} = \theta_{02}$ HORIZONTAL DISTANCE TRAVERSED BY THE DEGREE RAY IN THE LAYERS BELOW THE SOURCE.

$R_{\theta_{01}} = \theta_{01}$ HORIZONTAL DISTANCE TRAVERSED BY THE DEGREE RAY IN THE LAYERS BELOW THE SOURCE.
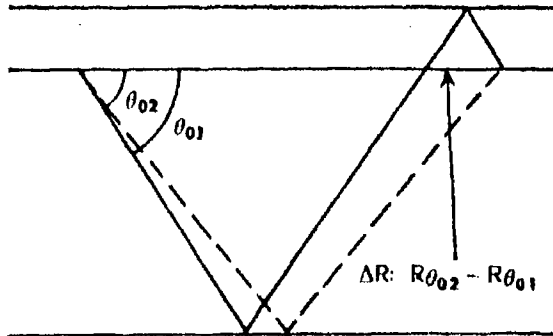
Fig. 2 - Geometry for Two Bottom-Reflected Rays

and the receiver at the same depth (see Fig. 2). The method applies, however, to rays with turning points and to cases where the source and the receiver are at different depths.

Assume that the range and its derivatives with respect to θ_o have been calculated for the θ_{01} degree ray. The problem is to find the travel-time difference and, hence, the phase difference between the rays.

Break the travel-time differences into two parts, one part being the time taken by the θ_{01} degree ray to traverse the layer above the source and the other being the difference in travel time between the two rays in the layers below the source and the receiver.

$$R = \sum_1^N (c_o/g_i \cos \theta_o)(\sin \theta_i - \sin \theta_{i+1}) , \quad (10)$$

$$T = \sum_1^N (1/g_i)$$
$$\times (\tanh^{-1} \sin \theta_i - \tanh^{-1} \sin \theta_{i+1}) , \quad (11)$$

$$dT/dR = (dT/d\theta_o)(d\theta_o/dR) = \cos \theta_o/c_o . \quad (12)$$

Expand T in a Taylor series as a function of R (below the receiver).

$$T\theta_{02} = T\theta_{01} + (R\theta_{02} - R\theta_{01})(dT/dR)$$
$$\quad (13)$$
$$+ (R\theta_{02} - R\theta_{01})^2/2 (d^2T/dR^2) + \ldots ,$$

$$T\theta_{02} - T\theta_{01} = \Delta R (dT/dR)$$
$$\quad (14)$$
$$+ [(\Delta R)^2/2] (d^2T/dR^2) + \ldots ,$$

where

$$d^2T/dR^2 = -(\sin \theta_o/c_o)(d\theta_o/dR) .$$

Equation (14) is the difference in travel time between the two rays in the layers below the source and the receiver, and this is an increase for the θ_{02} degree ray over the θ_{01} degree ray since dT/dR is always positive. In the layer above the receiver there is an increase in travel time for the θ_{01} degree ray over the θ_{02} degree ray. Thus, the total difference in travel time is

$$T_s\theta_{01} - (T\theta_{01} - T\theta_{02}) = \Delta T ,$$

where $T_s\theta_{01}$ is the travel time for the θ_{01} degree ray in the layer above the source.

It was found that for most cases the first term of the expansion was sufficient and that in the layers below the source and the receiver, the expression

$$T\theta_{01} - T\theta_{02} = \Delta R (\cos \theta_o/c_o)$$

was usually accurate.

Figure 3 shows theoretical plots of spreading loss versus range for signals reflected once from the bottom and for those reflected twice. The curves are based on intensities computed by using the formulas given above and the velocity-depth structure which existed at the time the measure-
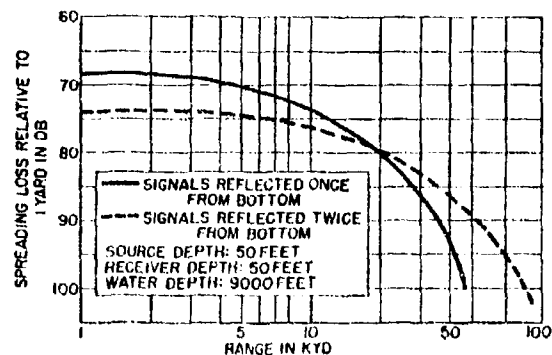

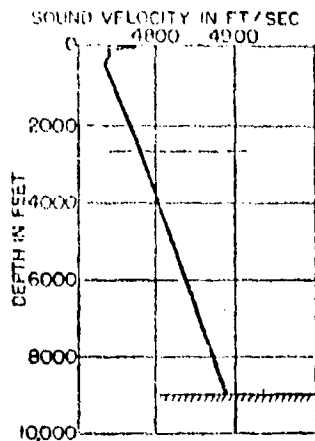
Fig. 3 - Theoretical Spreading-Loss Curves

Fig. 4 - Sound-Velocity—Depth Profile

ments were made. The velocity-depth profile for these measurements is shown in Fig. 4. The station was made at 75° north latitude and 01° east longitude during July.

In a homogeneous medium the two curves would approach a slope of 6 db per distance doubled as the slant range approached the horizontal range. However, for the station under consideration and for most deep-water locations there is considerable curvature for rays which make small angles with the bottom. As a result of this curvature, the
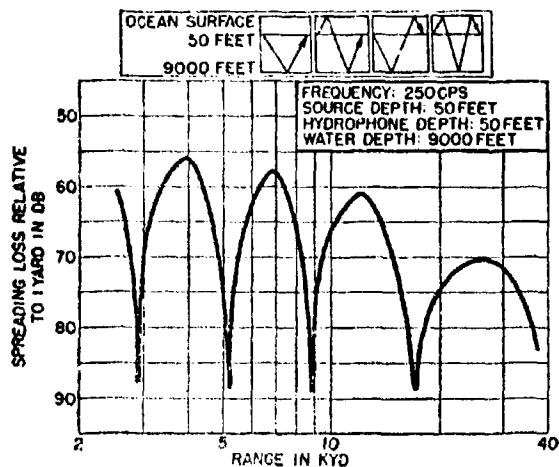
Fig. 5 - Spreading Loss for the Combined Four Signal Paths Reflected Once from the Bottom for a Frequency of 250 cps

rate of spreading loss is greater than 6 db at the longer ranges. For each of these orders of bottom reflection, as well as for all higher orders, there are four paths by which a signal can reach a receiver (see Fig. 5). For most of the ten bands into which the siren spectrum was resolved, the four signals could be combined simply by multiplying the intensity for one path by four. At the lower frequencies, however, the rate of change of phase with range was slow enough so that if phase were neglected, significant errors in the theoretical curve would result. The plot shown in Fig. 5 combines the four indicated paths for a frequency of 250 cps, which is the fundamental frequency of the siren used in the measurements. The source and the receiver are at depths of 50 feet, and the water depth is 9000 feet. Figure 6 presents a similar plot
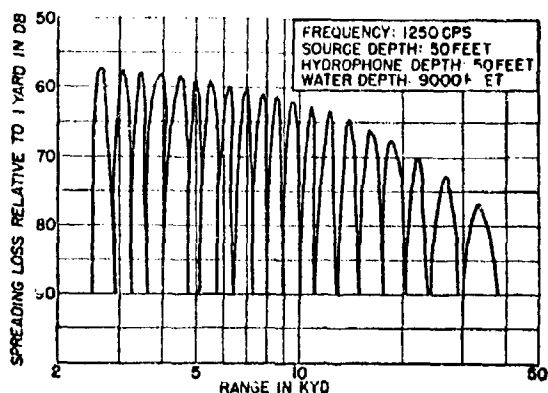

Fig. 6 - Spreading Loss for the Combined Four Signal Paths Reflected Once from the Bottom for a Frequency of 1250 cps

for the fifth harmonic of the siren. Because of the proximity of the peaks at this frequency and because there were two or more harmonics in the pass band of all the filters used in processing the data above the third harmonic, phase above this frequency was neglected.

The next step in the analysis was the construction of a theoretical curve which indicated loss versus range. The computations for this purpose included absorption and spreading for each of the ten frequency bands.[4] When the spreading loss

[4] Absorption was computed from Leonard's formula and by using the new constants which are presented by H. Wysor Marsh, Jr., and Morris Schulkin in Study A of this report.
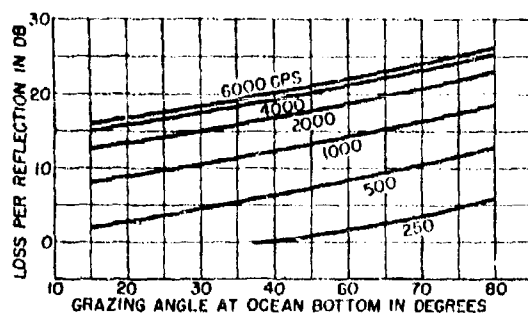
80

Fig. 7 - Reflection Loss vs. Grazing Angle at Ocean Bottom

Fig. 8 - Sound Pressure Level vs. Range for a Frequency of 250 cps

and absorption had been established as functions of range, the theoretical plots for signals reflected once from the bottom were compared with the measured propagation plots at short ranges where spreading predicted that these signals would be much stronger than those of higher-order reflection. A smoothed curve of loss per reflection versus angle of reflection at the bottom was then constructed for each of the ten frequency bands and extrapolated to include angles from 15° to 80°. Some of these curves are shown in Fig. 7 and indicate that the reflection loss increases with frequency and angle of reflection. The maximum range used in determining the curves was 10 kyd, which corresponded to a reflection angle of 30° for this station. Values from these curves were used to correct signals of higher-order bottom reflection, and the various orders were combined. The end result was a predicted curve which included spreading, absorption, and boundary loss for each frequency band.

In order to check these results, the predicted curves of level versus range were compared with the observed plots with the view that any large error in bottom-reflection loss would show up beyond the 10-kyd range, the maximum range used in determining the curves in Fig. 6. The agreement between the predicted and observed levels was good except for the 250-cps plot. This plot indicated that the bottom-reflection loss is not zero for angles of less than 37° (see Fig. 8). In Fig. 8 the solid curve is the predicted one. It is evident from Fig. 7 that the decrease in observed signal is more rapid than that expected if the loss were zero for grazing angles of less than 37°. Points beyond 26 kyd have been omitted because focused rays which do not reflect from the bottom arrive in

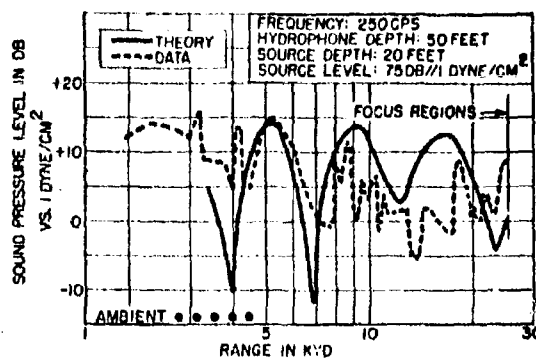this region. A sample of the good agreement at other frequencies is shown in Fig. 9, which is a plot of measured acoustic-pressure level versus range for the frequency band from 4000 to 5000 cps. The smooth curve is the one predicted on the basis of the bottom-reflection losses shown in Fig. 7.

Two focus regions, one at a range of 30 kyd and one at a range of 60 kyd, were observed during this station. These were caused by rays with initial source angles of less than approximately 12° which went through turning points at depths between 6000 and 9000 feet. As a result, four caustics were formed at shallow depths in both focus regions; each caustic was associated with one of the four possible paths. Because of the rapid convergence of the rays in the caustic region and the subsequent interference between neighboring rays, it was necessary to correct the levels based on
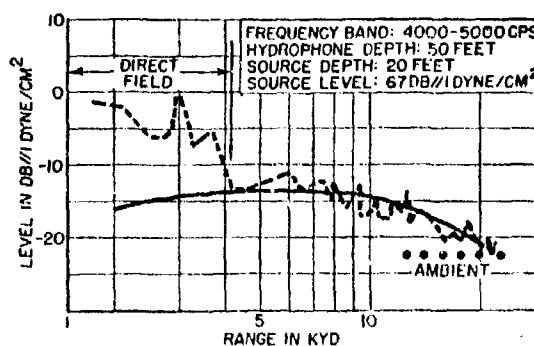

Fig. 9 - Sound Pressure Level vs. Range for the 4000- to 5000-cps Frequency Band
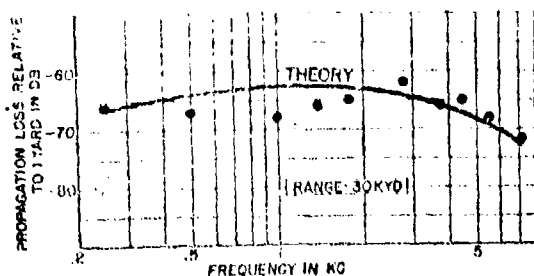
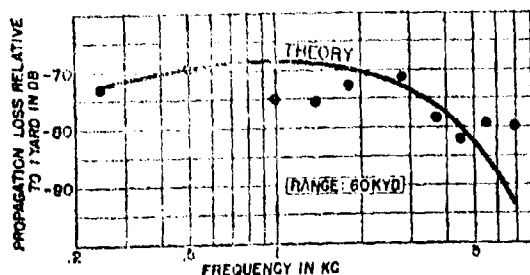Fig. 10 - Measured Propagation Loss to First Focus Region

Fig. 11 - Measured Propagation Loss to Second Focus Region

ray geometry for diffraction. This correction was accomplished by using the formulas given previously.

Figure 1, which is a graph of the correction factor for diffraction, predicts that the maximum intensity does not occur at the caustic where the first derivative vanishes but at some nearby point, the position of which is dependent on frequency. This fact is in agreement with the findings of Airy. By means of these corrections and by application of absorption loss, a theoretical curve for minimum propagation loss versus frequency for each focus region was drawn.

The curve for the first focus region near 30 kyd is shown in Fig. 10. This curve indicates a minimum loss of approximately 62 db at a frequency of 1500 cps which is caused by less intense focusing at the lower frequencies and higher absorption at the upper frequencies. Since the ambient level is lower and the bottom-reflected field drops to the ambient more quickly at higher frequencies, there is an argument for choosing one of the higher frequencies when attempting to observe the focusing phenomenon.

The predicted and observed propagation losses for the second focus region near 60 kyd are shown in Fig. 11. Although some scatter is apparent, there is good general agreement between the predicted and observed values. The peak of the theoretical curve appears at approximately 1000 cps as opposed to 1500 cps in Fig. 10. This fact indicates that as the range to the focus region increases, absorption will cause the optimum focus to shift toward increasingly lower frequencies. The scatter in Figs. 10 and 11 may well be an error in source level.

In conclusion, the complete intensity profile for one of the AMOS low-frequency noisemaker runs has been calculated according to the oceanographic picture. It has been possible to calculate the peak intensity in the focus region within a few decibels of the observed intensity. Bottom-reflection losses have been obtained as a function of the angle of reflection at the bottom. It remains now to check whether the behavior of other AMOS stations is similar to the behavior of the station discussed in this paper. Future plans also include a comparison of the bottom-reflection losses for each station with bottom cores and seismic profiles made during the measurements.

82

DOCUMENT CONTROL DATA - R & D

Security Classification of title, body of abstract and indexing annotation must be entered when the overall report is classified)

1. ORIGINATING ACTIVITY (Corporate author)	2a. REPORT SECURITY CLASSIFICATION
U. S. Navy Underwater Sound Laboratory Fort Trumbull, New London, Connecticut	UNCLASSIFIED
	2b. GROUP

3. REPORT TITLE

REPORT ON THE STATUS OF PROJECT AMOS (ACOUSTIC, METEOROLOGICAL, AND OCEANOGRAPHIC SURVEY) (1 JANUARY 1953 -- 31 DECEMBER 1954)

4. DESCRIPTIVE NOTES (Type of report and inclusive dates)
Research Report

5. AUTHOR(S) (First name, middle initial, last name)
H. Wysor Marsh, Jr.
Morris Schulkin

6. REPORT DATE	7a. TOTAL NO. OF PAGES	7b. NO. OF REFS
9 May 1967	61	25

8a. CONTRACT OR GRANT NO.	9a. ORIGINATOR'S REPORT NUMBER(S)
b. PROJECT NO.	255A
c.	9b. OTHER REPORT NO(S) (Any other numbers that may be assigned this report)
d.	

10. DISTRIBUTION STATEMENT

Distribution of this document is limited to DDC users.

11. SUPPLEMENTARY NOTES	12. SPONSORING MILITARY ACTIVITY
Unclassified edition of USL Report 255	U. S. Navy

13. ABSTRACT

This report is an UNCLASSIFIED edition of USL Report No. 255 (CONFIDENTIAL) dated 21 March 1955. The Project AMOS work which was carried out through the period 1 January 1953-31 December 1954 is summarized. This is a final report of the AMOS deep-water acoustic measurements, which began in June 1949. During the period covered by this report, the Underwater Sound Laboratory carried out a number of studies and analyses of AMOS data; these are included herein as Studies A through D and H through J.

The major study is an analysis of sound transmission at frequencies between 2 and 25 kc based on all the AMOS data and on other data available in the literature. Propagation-loss prediction charts based on this analysis are presented as a function of certain environmental parameters. An error study of the propagation analysis is presented next. Studies of AMOS low-frequency noisemaker data analysis, ray tracing in the ocean, and bottom reflection in deep water are also presented, and a summary of Cruise TWELVE, which was completed early in this period, is included.

DD FORM 1473 (PAGE 1)
1 NOV 65
S/N 0101-807-6801

UNCLASSIFIED
Security Classification

14 KEY WORDS	LINK A		LINK B		LINK C	
	ROLE	WT	ROLE	WT	ROLE	WT
Project AMOS						
Underwater Sound Transmission						
Sound Propagation Loss						
Underwater Sound Propagation						
Propagation Loss Prediction						
Bottom Loss						
Bottom Reflection						
AMOS Cruise 12						
Underwater Sound Transmission						
Transmission Loss						
Sonar Range Prediction						

DD FORM 1473 (BACK)
1 NOV 65
(PAGE 2)

UNCLASSIFIED
Security Classification

Navy Underwater Sound Laboratory
Report No. 255A
REPORT ON THE STATUS OF PROJECT AMOS
(ACOUSTIC, METEOROLOGICAL, AND OCEANOGRAPHIC
SURVEY) (1 JANUARY 1953 - 31 December 1954), by
H. Wysor Marsh, Jr. and Morris Schulkin. 9 May 1967.
i-iv + pp. 1-39 and 65-82, Figs.   UNCLASSIFIED
    This report is an UNCLASSIFIED edition of USL Report
No. 255 (CONFIDENTIAL), dated 21 March 1955. The
Project AMOS work which was carried out through the
period 1 January 1953 - 31 December 1954 is summarized.
This is a final report of the AMOS deep-water acoustic
measurements, which began in June 1949. During the
period covered by this report, the Underwater Sound

1. Underwater sound
   transmission —
   Measurement

I. Marsh, H. Wysor, Jr.
II. Schulkin, Morris
III. Project AMOS
IV. NE-120221-9

Laboratory carried out a number of studies and analyses
of AMOS data; these are included herein as Studies A
through D and H through J.
    The major study is an analysis of sound transmission
at frequencies between 2 and 25 kc based on all the
AMOS data and on other data available in the literature.
Propagation-loss prediction charts based on this analysis
are presented as a function of certain environmental
parameters. An error study of the propagation analysis
is presented next. Studies of AMOS low-frequency
noisemaker data analysis, ray tracing in the ocean, and
bottom reflection in deep water are also presented, and
a summary of Cruise TWELVE, which was completed
early in this period, is included.

1. Underwater sound
   transmission —
   Measurement

I. Marsh, H. Wysor, Jr.
II. Schulkin, Morris
III. Project AMOS
IV. NE-120221-9